© 2015. Published by The Company of Biologists Ltd | Journal of Cell Science (2015) 128, 3444-3455 doi:10.1242/jcs.170852

RESEARCH ARTICLE

Induction of lateral lumens through disruption of a monoleucine-based basolateral-sorting motif in betacellulin

Bhuminder Singh[1,2,3,*], Galina Bogatcheva[1,3], Alina Starchenko[2], Justine Sinnaeve[4], Lynne A. Lapierre[3,5], Janice A. Williams[6,7], James R. Goldenring[2,3,5,8] and Robert J. Coffey[1,2,3,8]

ABSTRACT

Directed delivery of EGF receptor (EGFR) ligands to the apical or basolateral surface is a crucial regulatory step in the initiation of EGFR signaling in polarized epithelial cells. Herein, we show that the EGFR ligand betacellulin (BTC) is preferentially sorted to the basolateral surface of polarized MDCK cells. By using sequential truncations and site-directed mutagenesis within the BTC cytoplasmic domain, combined with selective cell-surface biotinylation and immunofluorescence, we have uncovered a monoleucine-based basolateral-sorting motif (EExxxL, specifically ^{156}EEMETL^{161}). Disruption of this sorting motif led to equivalent apical and basolateral localization of BTC. Unlike other EGFR ligands, BTC mistrafficking induced formation of lateral lumens in polarized MDCK cells, and this process was significantly attenuated by inhibition of EGFR. Additionally, expression of a cancer-associated somatic BTC mutation (E156K) led to BTC mistrafficking and induced lateral lumens in MDCK cells. Overexpression of BTC, especially mistrafficking forms, increased the growth of MDCK cells. These results uncover a unique role for BTC mistrafficking in promoting epithelial reorganization.

KEY WORDS: Betacellulin, EGFR signaling, Epithelial polarity, Lateral lumens, MDCK cells, Polarized trafficking

INTRODUCTION

In the intact organism, most epithelia are organized as a single layer of cells lining organs, glands and body cavities. These cells are organized into discrete apical and basolateral compartments that are necessary to sense and respond to spatially restricted physical, chemical and microbial stimuli (Bryant and Mostov, 2008; Mellman and Nelson, 2008; Rodriguez-Boulan and Macara, 2014). EGF receptor (EGFR) signaling plays a vital role in epithelial homeostasis (Vermeer et al., 2003). Although EGFR is largely restricted to the basolateral surface, approximately 10% of EGFRs are present on the apical surface, and EGFR signaling from apical and basolateral surfaces can differ (Singh et al., 2013). EGFR activation is dependent on the binding of one of seven ligands – EGF, transforming growth factor-α (TGFA), amphiregulin (AREG), epiregulin (EREG), heparin-binding EGF-like growth factor (HBEGF), betacellulin (BTC) or epigen (EPGN) (Harris et al., 2003). All of these ligands are synthesized as type 1 transmembrane precursors. Proteolytic cleavage within the ectodomain releases the mature soluble ligand that binds to the receptor and initiates a complex cascade of downstream signaling events (Singh and Coffey, 2014b).

We have previously characterized the trafficking of EGF, TGFA, AREG and EREG in polarized epithelial cells (Dempsey et al., 2003, 1997; Gephart et al., 2011; Singh et al., 2013; Singh and Coffey, 2014a,b). These studies have established that spatially controlled ligand trafficking regulates EGFR activity. For example, EGF is delivered to both the apical and basolateral surfaces, but is preferentially cleaved from the basolateral surface (Dempsey et al., 1997). Basolateral EGF delivery is dependent on a PxxP motif (where x denotes any amino acid) within its cytoplasmic domain (Groenestege et al., 2007). TGFA, AREG and EREG are delivered to the basolateral surface; however, each is dependent on a distinct basolateral-sorting motif within their cytoplasmic domains. TGFA basolateral sorting depends on a dileucine motif and a cysteine-containing positively-charged juxtamembrane region (HCCQVRKH) (Dempsey et al., 2003). Basolateral sorting of AREG depends on a monoleucine-based motif (EExxxL), whereas a YxxΦ motif directs basolateral-cell-surface delivery of EREG (Brown et al., 2001; Gephart et al., 2011; Singh et al., 2013).

Despite the wealth of information that exists regarding BTC expression and function (Dahlhoff et al., 2014), its distribution in polarized epithelial cells is unknown. We now report that BTC localizes preferentially to the basolateral surface of polarized MDCK cells under steady-state conditions. Like AREG, sorting of BTC to the basolateral surface depends on a monoleucine-based sorting motif (EExxxL) (Gephart et al., 2011). Like TGFA, BTC also has a bipartite sorting motif; in addition to a dominant EExxxL motif, a cysteine-rich juxtamembrane region also contributes to BTC basolateral sorting (Dempsey et al., 2003). We also show that a cancer-associated somatic BTC mutation (E156K) results in loss of basolateral-sorting specificity. A unique feature of BTC mistrafficking, compared to the other EGFR ligands studied, is a significant increase in the number and size of lateral lumens in MDCK cells cultured on Transwell inserts and in three dimensions, a process that is, at least in part, dependent on EGFR activity.

RESULTS

BTC localizes to the basolateral surface of polarized MDCK cells

To examine the steady-state cell-surface distribution of BTC, we fused enhanced green fluorescent protein (EGFP) to the C-terminus of the human BTC coding sequence and stably expressed this chimera (BTC–EGFP) in polarized MDCK-II cells, hereafter referred to as MDCK cells (Fig. 1A). Confocal projections of polarized

[1]Department of Medicine, Vanderbilt University School of Medicine, Nashville, TN 37232, USA. [2]Department of Cell and Developmental Biology, Vanderbilt University School of Medicine, Nashville, TN 37232, USA. [3]Epithelial Biology Center, Vanderbilt University School of Medicine, Nashville, TN 37232, USA. [4]Interdisciplinary Graduate Program, Vanderbilt University School of Medicine, Nashville, TN 37232, USA. [5]Department of Surgery, Vanderbilt University School of Medicine, Nashville, TN 37232, USA. [6]Vanderbilt Ingram Cancer Center, Vanderbilt University School of Medicine, Nashville, TN 37232, USA. [7]Cell Imaging Shared Resource, Vanderbilt University School of Medicine, Nashville, TN 37232, USA. [8]Department of Veteran Affairs Medical Center, Nashville, TN 37232, USA.

*Author for correspondence (bhuminder.singh@vanderbilt.edu)

Received 2 March 2015; Accepted 5 August 2015

Journal of Cell Science (2015) 128, 3444-3455 doi:10.1242/jcs.170852

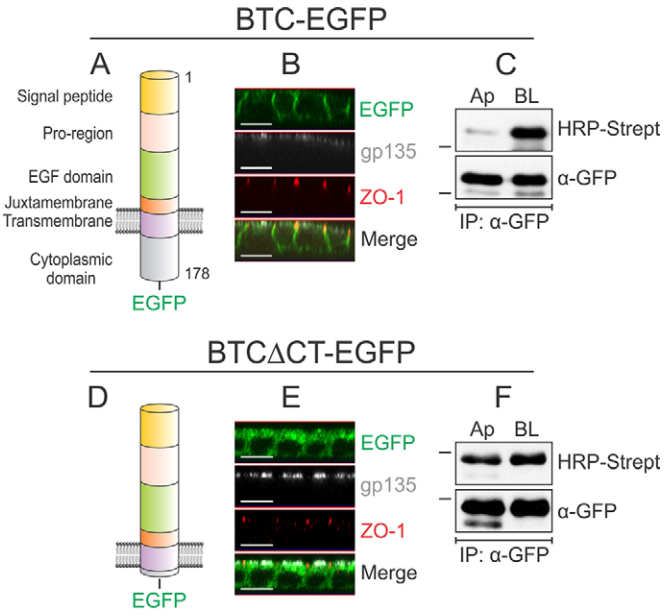

Fig. 1. Localization of BTC to the basolateral surface depends on its cytoplasmic domain. (A) Domain organization of human BTC. The 178-amino-acid pre-propeptide contains a 31-amino-acid signal peptide, a 33-amino-acid pro-region, a 41-amino-acid EGF domain, a 13-amino-acid juxtamembrane domain, a 21-amino-acid transmembrane domain and a 39-amino-acid cytoplasmic domain. The soluble 80-amino-acid BTC (residues 32–111) comprises the pro-region, EGF domain and part of the juxtamembrane region. (B) MDCK cells stably expressing BTC–EGFP were grown on Transwell filters for 5 days and were then paraformaldehyde-fixed and immunostained for ZO-1 (red) and gp135 (white); BTC–EGFP fluorescence is shown in green. Confocal projections in the *xz* plane are shown. (C) Polarized MDCK cells stably expressing BTC–EGFP were subjected to selective cell-surface biotinylation on either the apical (Ap) or basolateral (BL) surfaces. Cells were then lysed and immunoprecipitated (IP) with an anti-GFP antibody (α-GFP), and proteins were resolved on SDS-PAGE gels and probed with HRP–streptavidin to measure the extent of biotinylation on each surface (upper panel). Reblotting for GFP (lower panel) confirmed equal loading. (D) A construct lacking the distal 35 amino acids of the 39-amino-acid cytoplasmic domain is designated BTCΔCT–EGFP. (E) MDCK cells stably expressing BTCΔCT–EGFP were processed as cells described in B and immunostained for ZO-1 (red) and gp135 (white). (F) MDCK cells stably expressing BTCΔCT–EGFP were subjected to selective cell-surface biotinylation and displayed as described in C. All experiments were performed at least three times; representative images and blots are shown here. Dashes on the left of western blots indicate a molecular mass of 55 kDa. Scale bars: 10 µm.

MDCK cells expressing BTC–EGFP showed that cells displayed predominantly basolateral GFP fluorescence (Fig. 1B). GFP fluorescence was largely detected below ZO-1 immunoreactivity, a tight junction marker, and did not colocalize with gp135, an apical cell surface protein. Domain-selective cell-surface biotinylation followed by GFP immunoprecipitation and horseradish peroxidase (HRP)–streptavidin western blotting analyses showed that approximately 88% of BTC–EGFP was found at the basolateral surface (Fig. 1C, Fig. 2B). Thus, based on both immunofluorescence and selective cell-surface biotinylation, we show that BTC localizes predominantly to the basolateral cell surface under steady-state conditions.

BTC basolateral-sorting specificity resides within its cytoplasmic domain

Previous work from our lab has shown that the basolateral-sorting information of TGFA, AREG and EREG is contained within their respective cytoplasmic domains (Dempsey et al., 2003; Gephart et al., 2011; Singh et al., 2013). The 39-amino-acid cytoplasmic domain of BTC is highly conserved across species (supplementary material Fig. S1A). Upon removal of the terminal 35 amino acids, the resultant EGFP chimera (BTCΔCT–EGFP) showed similar GFP fluorescence intensity at both the apical and basolateral surfaces (Fig. 1D,E). Likewise, the BTCΔCT–EGFP protein was equally distributed between the apical and basolateral cell surfaces, as determined by using selective cell-surface biotinylation (Fig. 1F). These data indicate that, as expected, the basolateral-sorting specificity of BTC resides within its cytoplasmic domain.

Determination of region(s) within the BTC cytoplasmic domain that confer basolateral-sorting specificity

We next sought to determine which region(s) within the cytoplasmic domain of BTC confer basolateral-sorting specificity. We sequentially removed five amino acids from the C-terminus, generating eight truncation mutants, which were fused to EGFP at their carboxyl termini (CT1 to CT8, Fig. 2A). Removal of up to 15 amino acids from the cytoplasmic domain did not affect basolateral sorting of BTC (CT1, CT2 and CT3); the slight reduction in basolateral sorting that we observed for these constructs was not significantly different from wild-type BTC (Fig. 2B). However,

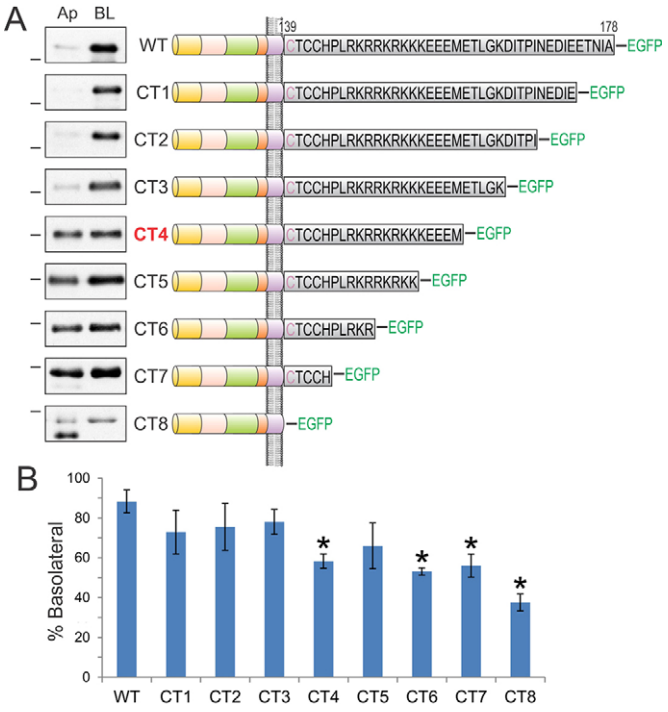

Fig. 2. Analysis of sequential cytoplasmic domain truncations of BTC identifies its basolateral-sorting regions. (A) The BTC cytoplasmic domain is expanded to display the individual 39 amino acids in black. BTC is palmitoylated within the juxtamembrane CTCC motif; the first cysteine residue (depicted in purple) is predicted to reside within the transmembrane domain. Polarized MDCK cells stably expressing successive 5-amino-acid BTC truncations fused to EGFP at the C-terminus (CT1 to CT8) were subjected to selective cell-surface biotinylation on apical (Ap) or basalolateral (BL) cell surfaces. Note that the results for CT7 are shown as BTCΔCT–EGFP in Fig. 1F. Cellular lysates were harvested and subjected to GFP immunoprecipitation, and proteins were resolved on SDS-PAGE and then probed with HRP–streptavidin to measure the extent of biotinylation, which is displayed in the panel on the left. Dashes on the left of western blots indicate a molecular mass of 55 kDa. (B) Quantification of western blots. % Basolateral=([BL]/[Ap]+[BL])×100. Combined results from at least three independent experiments are represented as mean±s.e.m., *statistically significant difference ($P<0.05$, two-tailed unpaired *t*-test) compared with wild type.

Journal of Cell Science (2015) 128, 3444-3455 doi:10.1242/jcs.170852

removal of an additional five amino acids (CT4) compromised basolateral sorting, leading to equivalent distribution of the truncated protein at the apical and basolateral cell surfaces. Subsequent truncations [CT5, CT6 and CT7 (referred to as BTCΔCT in Fig. 1)] continued to display loss of polarized trafficking. Basolateral abundance of CT4, CT5, CT6 and CT7 was 58%, 66%, 53% and 56%, respectively; of these, CT4, CT6 and CT7 significantly compromised basolateral sorting compared to that of wild-type BTC (Fig. 2B). BTC is palmitoylated at juxtamembrane cysteine residues (Stoeck et al., 2010). CT8, which lacks the entire cytoplasmic domain, including these cysteine residues, showed the largest disruption of polarized BTC distribution with predominant apical localization – only 37% was present at basolateral surface. We observed two major cell surface forms for most BTC constructs, which are likely to represent different post-translational modifications, such as glycosylation (Fig. 1C,F). For the CT8 mutant, the faster migrating cell-surface form showed predominantly apical localization (Fig. 2, CT8 panel).

BTC contains a monoleucine-based basolateral sorting motif (EExxxL)

We have previously described a monoleucine-based basolateral sorting motif (EExxxL) in AREG (Gephart et al., 2011). The BTC cytoplasmic domain also contains this motif (^{156}EEMETL^{161}), which is highly conserved across species (supplementary material Fig. S1A). A BTC cytoplasmic domain truncation mutant, CT4, which lacks the leucine residue within this motif, shows a non-polar cell-surface distribution (Fig. 2). When we mutated the conserved amino acids within this motif to alanine, alone or in combination in full-length BTC [E156A (E>A); E156A E157A (EE>AA); L161A (L>A); and E156A E157A L161A, triple mutant (TM)], the resulting mutants showed equivalent localization at the apical and basolateral cell surfaces (Fig. 3A). The basolateral abundances of L>A, E>A, EE>AA and TM were 55%, 44%, 46% and 46%, respectively (Fig. 3B). Thus, the EExxxL motif is required for the efficient basolateral sorting of BTC. Notably, an EExxxL motif is also present in another basolateral EGFR ligand, HBEGF. After sequence alignment of AREG, BTC and HBEGF, we found that the leucine and proximal acidic amino acids within this motif are conserved in all three ligands (supplementary material Fig. S1B).

Compared to the CT7 truncation, the CT8 deletion, which removes the cysteine-rich motif (CTCC), further disrupted BTC basolateral-sorting specificity (Fig. 2). It has previously been shown that BTC undergoes palmitoylation at these cysteine residues (Stoeck et al., 2010). To assess the role of these cysteine residues in the cell-surface distribution of BTC, we mutated all of these cysteine residues to alanine in the context of full-length BTC. The resultant C3 mutant showed a predominant basolateral cell-surface distribution (Fig. 3). However, when the C3 mutant was combined with the TM mutant (C3/TM), there was a further reduction in BTC basolateral localization compared to that of the TM mutant alone (80% of C3 vs 36% of C3/TM at the basolateral surface, Fig. 3B), suggesting that both motifs contribute to basolateral-sorting specificity.

We next considered other post-translational modifications that might affect polarized sorting of BTC. Within its extracellular domain, BTC contains an NxS/T sequon, a putative acceptor site for N-glycosylation, which is a recognized apical-sorting motif (Hobert et al., 1997; Scheiffele et al., 1995). Pre-incubating BTC with the N-glycosylation inhibitor tunicamycin resulted in a decrease in the molecular mass of BTC, confirming BTC N-glycosylation (supplementary material Fig. S1C). However, treatment with

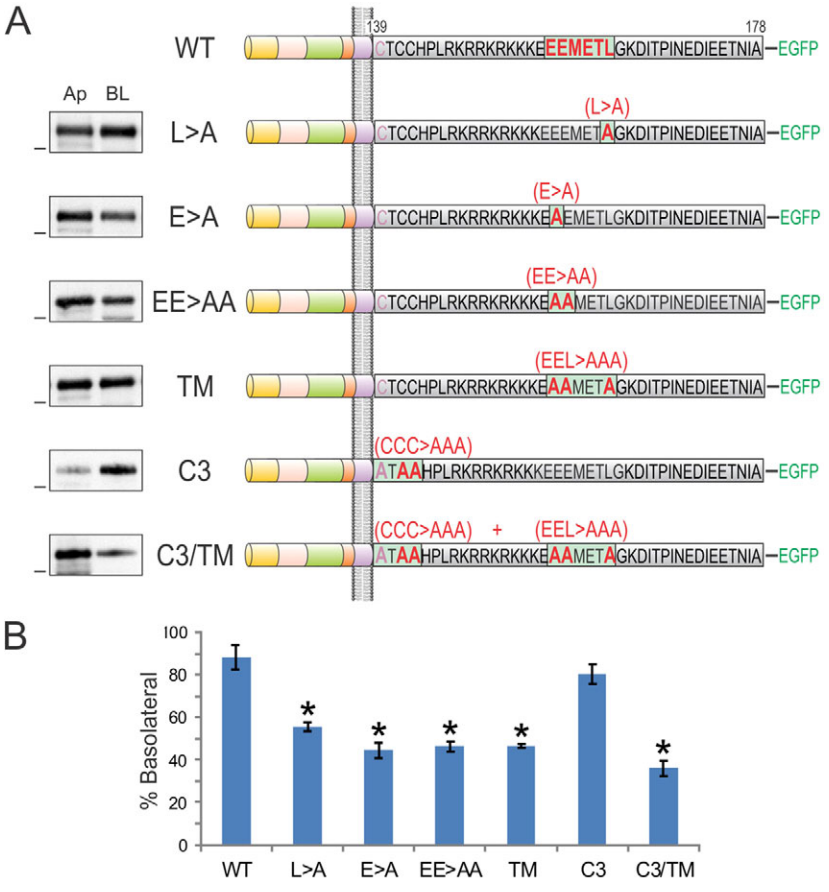

Fig. 3. The BTC cytoplasmic domain contains a monoleucine-based basolateral sorting motif (EExxxL). In the top panel, the wild-type BTC cytoplasmic domain sequence is depicted with a putative basolateral-sorting motif highlighted in red. In subsequent panels, amino acid substitutions within the cytoplasmic domain are displayed. Cell-surface biotinylation was performed as described in Fig. 2. TM, triple mutant in which the monoleucine and glutamic acid residues were converted to alanine; C3, all three juxtamembrane cysteine residues were converted to alanine. Dashes on the left of western blots indicate a molecular mass of 55 kDa. (B) Quantification of western blots. % Basolateral=([BL]/[Ap]+[BL])×100. Combined results from at least three independent experiments are represented as mean±s.e.m.; *statistically significant difference (P<0.05, two-tailed unpaired t-test) compared with wild type (WT). C3/TM, combined C3 and TM mutant.

Journal of Cell Science (2015) 128, 3444-3455 doi:10.1242/jcs.170852

tunicamycin did not alter the steady-state distribution of either wild-type BTC or triple mutants, as determined by using selective cell-surface biotinylation, indicating that N-glycosylation is not required for apical mislocalization of mutant BTC (supplementary material Fig. S1C).

Induction of lateral lumens in polarized MDCK cells through BTC mistrafficking

In addition to the expected gp135 immunoreactivity at the apical surface of fully polarized MDCK cells on Transwell filters, we observed patchy gp135 staining along the lateral membranes in MDCK cells that stably expressed the BTC mistrafficking mutant C3/TM (Fig. 4A). This lateral gp135 immunoreactivity was limited by a ZO-1 ring that was visible in *yz* slices and three dimensional (3D) reconstructions (Fig. 4A; supplementary material Movie 1). This ZO-1 ring was not continuous with the characteristic polygonal ZO-1 staining pattern that denotes apical tight junctions (Fig. 4A; supplementary material Movie 1). These patchy regions are reminiscent of lateral lumens that are observed in WIF-B cells and in MDCK cells overexpressing Par1b in conjunction with a Ca^{2+}

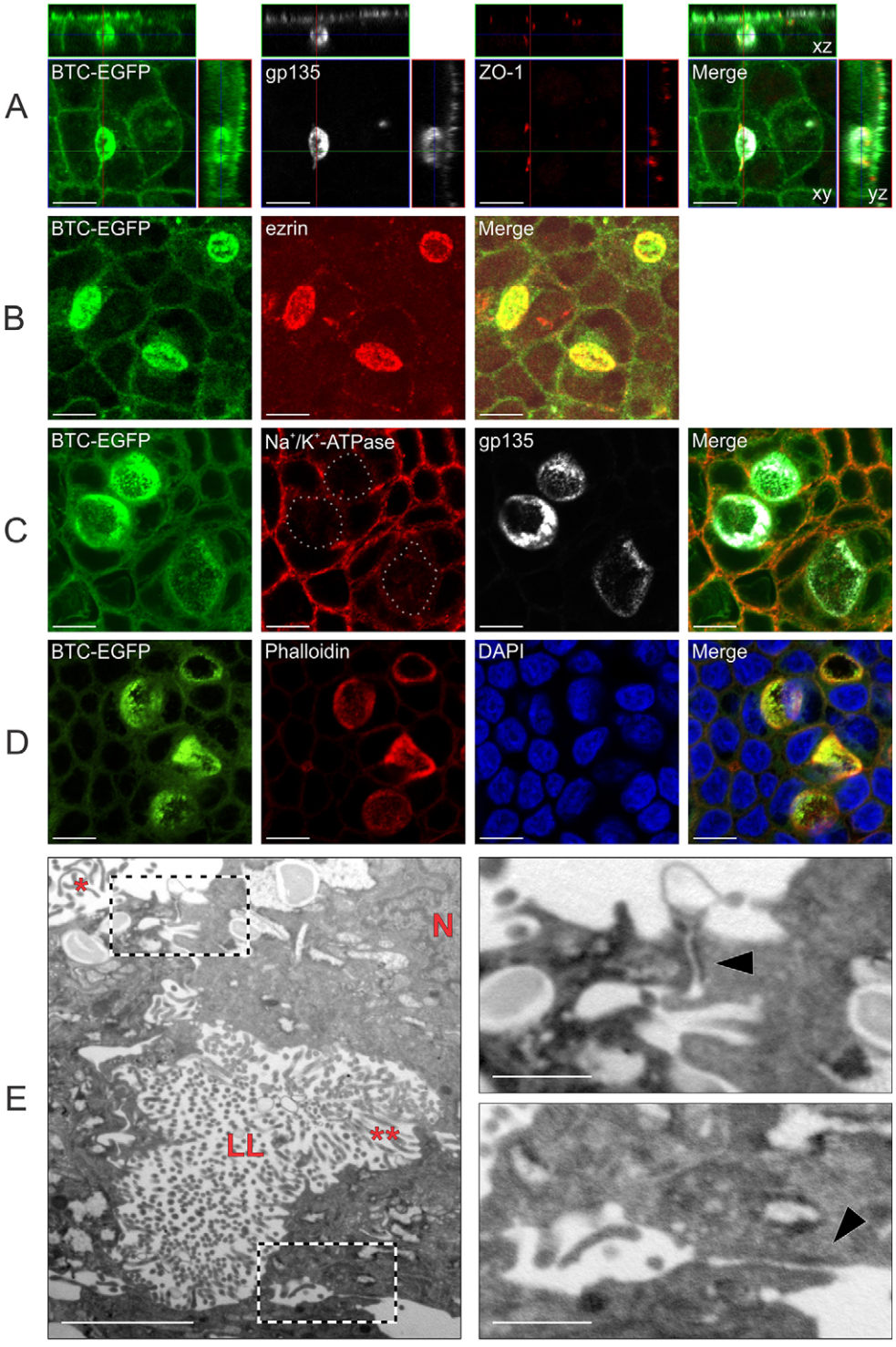

Fig. 4. BTC mistrafficking results in lateral lumen formation in polarized MDCK cells. (A–D) Polarized MDCK cells stably expressing (C3/TM)BTC–EGFP were fixed and stained with polarity markers. In A, immunofluorescence for gp135 (white) and ZO-1 (red) is shown with BTC–EGFP fluorescence (green). Confocal *xy* projections for each stain are shown in the center with *xz* and *yz* projections displayed to the top and right, respectively. In B, cells were stained for an apical marker, ezrin (red). In C, cells were stained for a basolateral marker, Na^+/K^+-transporting ATPase α1 subunit (red), and an apical marker, gp135 (white); in the second panel, lateral lumen membranes are highlighted with dotted lines. In D, cells were stained for Rhodamine–phalloidin (red) and for nuclei with DAPI (blue). (E) Polarized MDCK cells stably expressing (C3/TM)BTC–EGFP were fixed and processed for transmission electron microscopy analyses, as described in Materials and Methods. The main figure on the left shows lateral lumen (LL) with microvilli (**). Apical microvilli and nuclei are indicated with * and N, respectively. On the right, high-magnification views of the two boxed areas from the left panel show tight junctions (black arrowheads) above (top panel) and below (bottom panel) the lateral lumen. Scale bars: 10 µm (A–D); 2 µm (E, main image); 0.5 µm (E, insets).

Journal of Cell Science (2015) 128, 3444-3455 doi:10.1242/jcs.170852

switch or collagen overlay (Cohen et al., 2004; Cohen and Müsch, 2003). In the latter instance, gp135 only decorates the lateral-lumen-limiting membranes and not the membranes at the apex. By contrast, we observed gp135 immunoreactivity at both the apical surface at the apex and lateral-lumen-limiting membrane at the same time on the same cell (Fig. 4A). These lateral lumen membranes were enriched for F-actin and another apical protein, ezrin (Fig. 4B,D), and excluded the basolateral protein Na^+/K^+-transporting ATPase α1 subunit (Fig. 4C). The fluorescence associated with the C3/TM protein fused to GFP [(C3/TM)BTC–EGFP] also decorated lateral lumen membranes (Fig. 4A–D). Using transmission electron microscopy (TEM) imaging, we confirmed that lateral lumens were limited by tight junctions on the top and bottom, and further showed that they contained microvilli (Fig. 4E and insets). Organization of microtubules and actin stress fibers, as well as centriole localization, were similar in parental and (C3/TM)BTC–EGFP-expressing MDCK cells that were cultured on Transwell filters (supplementary material Fig. S2A,B,D,E). In dividing (C3/TM)BTC–EGFP-expressing MDCK cells, we occasionally observed one spindle pole that was oriented towards the lateral lumen (supplementary material Fig. S2C).

Lateral lumens form after establishment of apico-basolateral polarity, and apical proteins do not transcytose to lateral lumens

We next wanted to determine whether formation of lateral lumens preceded that of the apical domain at the apex. In a timecourse experiment, lateral lumens appeared at day 3 on Transwell cultures, and increased in size and area at days 4 and 5 (Fig. 5A). Older cultures also showed multilayering of the epithelium (Fig. 5B). The apical surface was detected at day 2 and was maintained through days 3 to 5, indicating that the apical surface forms before lateral lumens (Fig. 5B). Because lateral lumens were enriched for apical proteins and formed after the apical surface, we tested whether proteins from the apical surface are transcytosed to the lateral lumen membranes. However, after up to 5 h of chase of biotin–streptavidin-labeled apical proteins, we failed to detect streptavidin fluorescence within the lateral lumens (Fig. 5C; data not shown). These results suggest that apical proteins do not traffic to the lateral lumens through apical-to-lateral-lumen transcytosis.

Detection of lateral lumens in parental MDCK cells – selective enhancement by BTC mistrafficking

Upon careful inspection, we noted a small number of lateral lumens in parental MDCK cells; on average, four lateral lumens were observed per microscope field, which means that less than 1% of parental MDCK cells were associated with lateral lumens. There was a trend towards increased lateral lumen number and size upon overexpression of wild-type BTC–EGFP compared to parental MDCK cells, but this did not reach statistical significance. However, both parameters dramatically increased with overexpression of BTC mistrafficking mutants, both TM and C3/TM, compared with parental MDCK cells (Fig. 6A–D; supplementary material Movie 2). The number of lateral lumens and the area of the lumens were greater in the cells expressing the C3/TM combined mutant compared to those expressing the TM single mutant (Fig. 6A–C; supplementary material Movies 1, 3, 4). In addition to the effects on Transwell cultures, we also observed that mistrafficked BTC induced lateral lumens in 3D Matrigel cultures; (C3/TM)BTC–EGFP-expressing MDCK cells formed cysts that had a central lumen surrounded by multiple smaller lateral lumens, in contrast to the single central lumens that were observed for parental MDCK cells or BTC–EGFP-expressing MDCK cells (supplementary material Fig. S3). The induction of lateral lumens appeared to be specific for BTC because mistrafficked forms of AREG (mutant EEL2A, ^{156}EERKKL^{161} to ^{156}AARKKA^{161}) or EREG (Y156A) did not substantially affect lateral lumen formation (supplementary material Fig. S4) (Gephart et al., 2011; Singh et al., 2013).

In addition to the quantitative differences (lateral lumen number and size), we next tested whether BTC mistrafficking induced qualitative changes in the composition and architecture of lateral

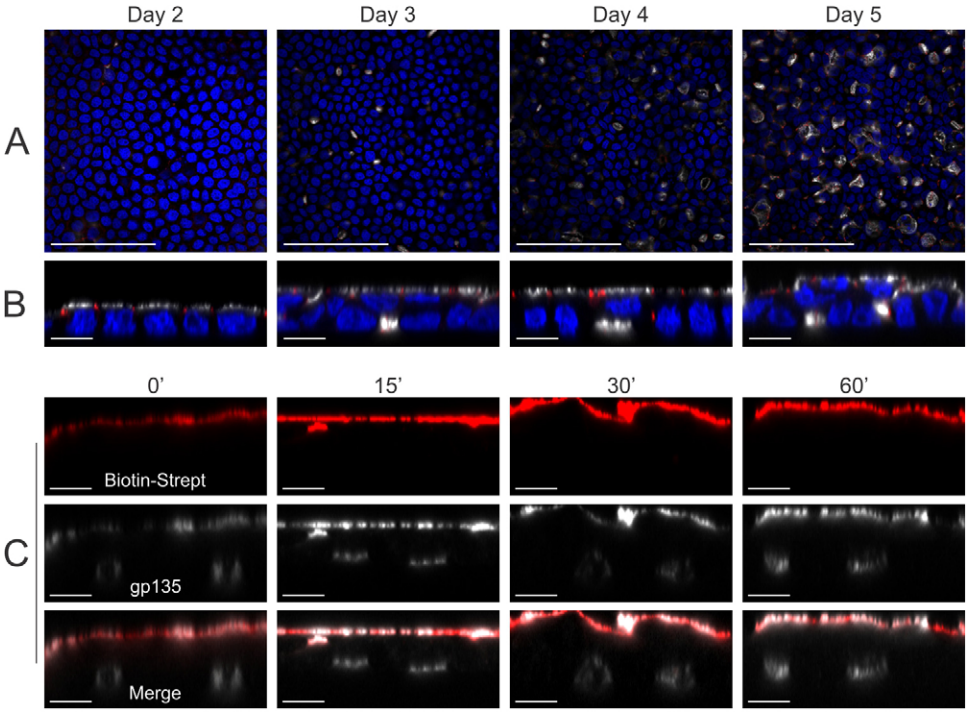

Fig. 5. Lateral lumens form after establishment of apico-basolateral polarity, and apical proteins do not transcytose to lateral lumens. (A,B) (C3/TM)BTC–EGFP-expressing MDCK cells were cultured on Transwell filters, fixed at the indicated times and then stained for DAPI (blue), gp135 (white) and ZO-1 (red); *xy* (A) and *xz* (B) projections show gp135- and ZO-1-decorated lateral lumens. (C) The apical cell surface of polarized MDCK cells stably expressing (C3/TM)BTC–EGFP was incubated with membrane-impermeable biotin, followed by labeling with Cy3–streptavidin (red) at 4°C. The labeled apical proteins were chased at 37°C for the indicated times (min), and cells were then fixed and stained for gp135 (white) to label apical surface and lateral lumens. *xz* projections of individual and merged channels are displayed here. Scale bars: 100 µm (A); 10 µm (B,C).

Journal of Cell Science (2015) 128, 3444-3455 doi:10.1242/jcs.170852

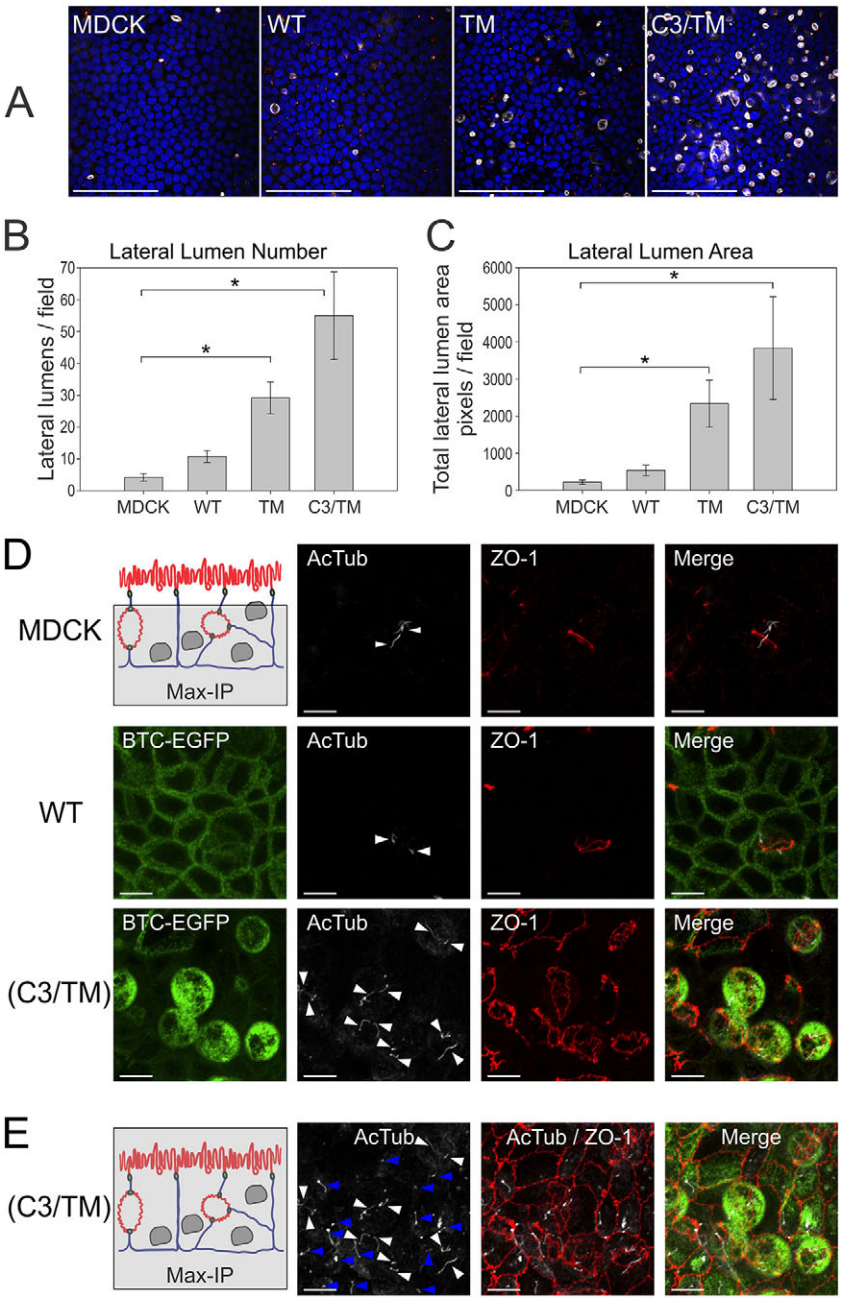

Fig. 6. Detection of lateral lumens in polarized MDCK cells – enhancement by BTC mistrafficking. (A) Parental MDCK cells and MDCK cells stably expressing the indicated BTC constructs were polarized on Transwell filters, and then fixed and stained with DAPI (blue), and for gp135 (white) and ZO-1 (red). Quantification of number (B) and area (C) of lateral lumens. *Statistically significant difference, $P<0.05$. See Materials and Methods for details. (D) Polarized MDCK cells expressing the indicated constructs were fixed and stained for acetylated tubulin (AcTub, white) and ZO-1 (red). Maximum intensity projections (Max-IP) of the *z*-stacks, excluding the apical surface, are displayed; the area included in the analysis is shaded in gray in the schematic at the top left. Individual primary cilia are indicated by white arrowheads. (E) Maximum intensity projections that include the apical surface at the apex (schematic on left) from the corresponding area imaged in D for (C3/TM)BTC–EGFP-expressing MDCK cultures are displayed. White arrowheads indicate primary cilia within the lateral lumens; blue arrowheads indicate apical primary cilia at the apex. In the schematics in D,E: red, apical surfaces; blue, basolateral membranes. WT, wild type. Scale bars: 100 µm (A); 10 µm (D,E).

lumens. We compared lateral lumens from parental MDCK cells and BTC–EGFP- and (C3/TM)BTC–EGFP-expressing MDCK cells. Lateral lumens from all three lines were encircled by a ZO-1 ring, and exhibited gp135 and ezrin immunoreactivity, but were devoid of staining for Na^+/K^+-transporting ATPase α1 subunit (Fig. 4B,C; supplementary material Movies 1–4). In addition, typically one or two, and occasionally more, primary cilia (as determined by staining for acetylated tubulin) were present in each lateral lumen from all three lines, indicating that each apical surface in lateral lumens contributes to one primary cilium (Fig. 6D). To our knowledge, this is the first demonstration of primary cilium in lateral lumens. The presence of cilia at the apical surface was undisturbed; lateral lumen cilia and apical cilia were present within the same field, as shown for (C3/TM) BTC–EGFP-expressing MDCK Transwell cultures; however, we did not observe the simultaneous presence of primary cilia on both apical surfaces in individual cells (Fig. 6E). Taken together, these data indicate that BTC mistrafficking increases the frequency of lateral lumens, but that the composition and architecture remain similar to those in parental MDCK monolayers.

EGFR activity contributes to lateral lumen formation

Given the role of BTC mistrafficking in the induction of lateral lumens, we examined the regulation of lateral lumen formation by mistrafficked BTC. The biological activity of BTC is primarily mediated by metalloproteinase-dependent cleavage and binding to its cognate receptors, EGFR and ERBB4 (Sahin et al., 2004). MDCK cells express approximately 40,000 EGFRs; the presence of ERBB4 has not been reported. We blocked EGFR activity with an irreversible EGFR tyrosine kinase inhibitor, EKI-785, to test whether altered EGFR signaling affected the lateral lumen formation induced by BTC mistrafficking (Discafani et al., 1999). Incubation with EKI-785

Journal of Cell Science (2015) 128, 3444-3455 doi:10.1242/jcs.170852

did not affect the sorting specificity of BTC; BTC–EGFP remained at the basolateral surface, and non-polarized sorting of the C3/TM mutants was unaltered. Incubation with EKI-785, however, significantly decreased the size and number of lateral lumens by more than 50% in (C3/TM)BTC–EGFP-expressing cells (Fig. 7A–C). Reduction of lateral lumen area and number was not statistically significant in BTC–EGFP-expressing cells after incubation with EKI-785 (Fig. 7B,C). The area of the lateral lumen in parental MDCK cells was also significantly reduced after incubation with EKI-785 (Fig. 7C). We next observed parental and (C3/TM)BTC–EGFP-expressing MDCK cells in a collagen-overlay assay, with the addition of collagen on top of the established epithelium. Within 2 days of collagen addition (which activates integrin signaling at the apex and provides a strong polarizing cue), parental MDCK monolayers transformed into a bilayer with the apical surfaces facing each other (Fig. 7D, upper panel). (C3/TM)BTC–EGFP-expressing MDCK cells, however, failed to form a clear bilayer and presented as multilayered structures instead; in these cells, bilayer structures were only achieved by inhibiting EGFR signaling through treatment with EKI-785, indicating an antagonistic relationship between EGFR and integrin signaling in this assay (Fig. 7D, lower panels). Taken together, these data suggest that mistrafficked BTC induces lateral lumen formation, a process that is dependent, at least in part, on EGFR signaling.

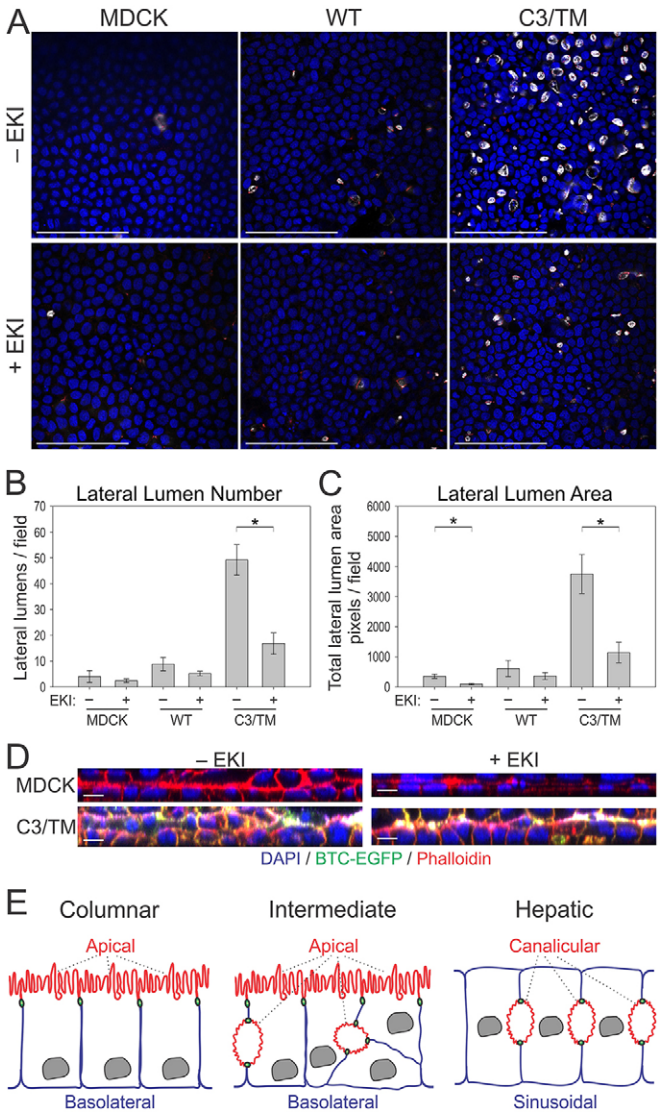

Fig. 7. EGFR activity contributes to lateral lumen formation. (A) Polarized MDCK cells stably expressing the indicated BTC constructs were treated with an irreversible EGFR tyrosine kinase inhibitor (EKI-785, 2 µM, +EKI) or diluent (−EKI) between days 3 and 5 of culture on Transwell filters. At day 5, the cells were fixed and stained with DAPI (blue), and for gp135 (white) and ZO-1 (red). Quantification of number (B) and area (C) of lateral lumens in MDCK cells stably expressing indicated constructs. *Statistically significant difference, $P<0.05$. See Materials and Methods for details. (D) Four-day-old parental and (C3/TM)BTC–EGFP-expressing MDCK Transwell cultures were overlaid with collagen in the presence or absence of 2 µM EKI-785 for an additional two days, and fixed and stained with DAPI (blue) and phalloidin (red); *xz* projections are displayed. (E) Schematic of different types of epithelial polarity. Columnar polarity is exemplified by MDCK cells, where the apical surface (red) is on top and is separated from the basolateral surface (blue) by intervening tight junctions (green). Another type of epithelial polarity is exemplified by hepatocytes, where the apposed canalicular membranes form the apical surface and the sinusoidal membranes are the functional equivalent of basolateral membranes. BTC mistrafficking (middle panel, intermediate) induces features of hepatic polarity, namely lateral lumens within a polarized columnar epithelium. Lateral lumens are separated from basolateral membranes by tight junctions. WT, wild type. Scale bars: 100 µm (A); 10 µm (D).

A human cancer-associated mutation (E156K) disrupts the BTC basolateral-sorting motif and specificity

Seventeen different mutations in the coding region of BTC have been reported in human cancers in the cBio cancer genomics portal (www.cbioportal.org) (Cerami et al., 2012; Singh and Coffey, 2014b). Two of these mutations (G101stop in lung adenocarcinoma and E156K in melanoma) are predicted to remove or disrupt the basolateral-sorting motif. Because E156K lies within the EExxxL motif in BTC, we generated the (E156K)BTC–EGFP mutant and expressed it stably in MDCK cells in order to observe its effect on the polarized sorting of BTC (Fig. 8A, schematic). (E156K)BTC–EGFP localized almost equally between apical and basolateral membranes (analyzed by using selective cell-surface biotinylation), confirming that this cancer-associated mutation disrupts the basolateral sorting of BTC (Fig. 8A). We also observed that (E156K)BTC–EGFP expression significantly increased the transepithelial electrical resistance (TEER); the TEER of BTC–EGFP- and (C3/TM)BTC–EGFP-expressing cells was virtually unperturbed; however, the significance of this difference is unknown (data not shown). Notably, (E156K)BTC–EGFP expression also increased the size and number of lateral lumens (Fig. 8B). However, the decrease in size and number of lateral lumens failed to reach statistical significance after treatment of these cells with EKI-785.

BTC mistrafficking confers a growth advantage

After observing altered epithelial characteristics (lateral lumens, multilayering), we compared the growth on Transwell cultures of MDCK cells that expressed different BTC constructs (Fig. 8E). Within 3 days of plating, both (C3/TM)BTC–EGFP- and (E156K) BTC–EGFP-expressing MDCK cells showed significantly higher growth than parental MDCK cells, which remained higher upon prolonged culturing. At day 3, the number of (C3/TM)BTC–EGFP-expressing cells was more than double (125%) that of the parental MDCK cells; a corresponding 56% increase was observed for (E156K)BTC–EGFP-expressing cells. Expression of wild-type BTC also increased MDCK growth, but it was significant only after day 5; at this time, only a 30% increase was observed.

DISCUSSION

Here, we show that the EGFR ligand BTC localizes preferentially to the basolateral surface of polarized MDCK cells. We have also

Journal of Cell Science (2015) 128, 3444-3455 doi:10.1242/jcs.170852

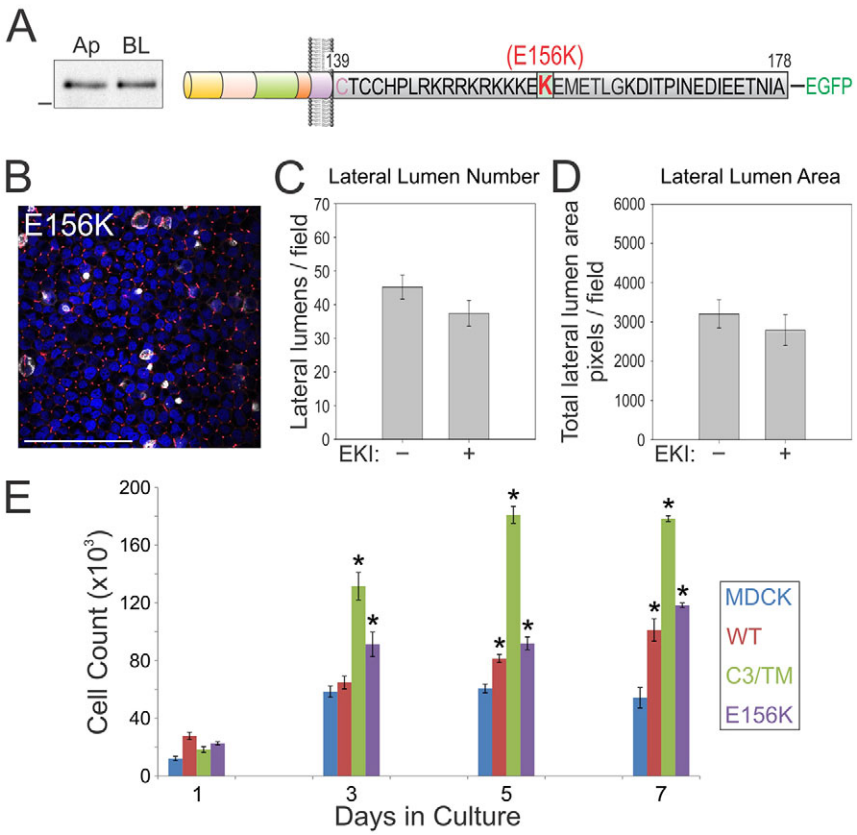

Fig. 8. A human cancer-associated somatic mutation in the BTC basolateral-sorting motif compromises basolateral trafficking. (A) The E156K BTC mutation that is associated with human pathology was generated within the full-length human BTC protein and fused with EGFP at its C-terminus (top schematic). The relative abundance of the E156K mutant at the apical (Ap) or basolateral (BL) cell surface, as determined by using selective cell-surface biotinylation, is depicted on the left. (B) MDCK cells stably expressing E156K BTC were polarized on Transwell filters, and then fixed and stained with DAPI (blue), and for gp135 (white) and ZO-1 (red). Scale bar: 100 µm. (C,D) E156K-expressing polarized MDCK cells were treated with EKI-785 (EKI) as in Fig. 6. Quantification of number (C) and area (D) of lateral lumens. (E) One hundred thousand MDCK cells stably expressing the indicated BTC–EGFP constructs were plated on Transwell filters in triplicate and counted at the indicated time points. Data are plotted as mean±s.e.m.; *statistically significant difference (P<0.05, two-tailed unpaired t-test) compared with parental MDCK cells. WT, wild type.

identified a monoleucine-based sorting motif and a cysteine-rich juxtamembrane region within the cytoplasmic domain that govern the basolateral localization of BTC. Disruption of these motifs results in loss of polarized BTC distribution and leads to the formation of lateral lumens in unperturbed polarized MDCK cultures. These lateral lumens are enriched for apical proteins, such as gp135, and contain microvilli and primary cilia. Such a phenotype was not observed in MDCK cells that stably expressed wild-type or mistrafficked forms of EGF, TGFA, AREG and EREG. In addition, we show that this process is, at least in part, dependent on EGFR tyrosine kinase activity.

Preferential sorting of BTC in polarized epithelial cells

All of the EGFR ligands studied, with the exception of EGF, showed preferential basolateral localization under steady-state conditions in polarized epithelial cells. EGF is delivered equally to both the apical and basolateral surface, but is selectively cleaved from the basolateral surface (Dempsey et al., 1997). In this study, we have shown that BTC is preferentially localized to the basolateral surface under steady-state conditions in polarized MDCK cells. Using C-terminal-truncation mutants and specific amino acid substitutions within the cytoplasmic domain, we have identified two regions that contribute to the basolateral sorting of BTC.

The dominant BTC basolateral-sorting information resides in the EExxxL motif. All three key residues – two proximal glutamates and a distal leucine – are absolutely required for the integrity of this motif because removal of any one leads to a similar disruption of apico-basolateral polarity to that of all three in combination; the mutations are not additive. There is strong conservation of amino acids upon cross-species alignment of this motif. In fact, both E156 and L161 are conserved in non-aquatic vertebrates that express BTC (supplementary material Fig. S1A). The monoleucine-based basolateral-sorting motif in the cytoplasmic domain of AREG is also highly conserved (Gephart et al., 2011). Interestingly, this motif is also present in HBEGF, another basolateral EGFR ligand, and we speculate that this motif might direct basolateral sorting of HBEGF (supplementary material Fig. S1B) (Nakamura et al., 1995; Singh and Coffey, 2014b). Thus, the EExxxL basolateral-sorting motif is the most common basolateral-sorting motif amongst the family of mammalian EGFR ligands; a PxxP motif in EGF, a dileucine motif in TGFA and a YxxΦ motif in EREG are represented only once (Dempsey et al., 2003; Gephart et al., 2011; Groenestege et al., 2007; Singh et al., 2013).

The EExxxL motif is involved in the biosynthetic basolateral delivery of AREG (Gephart et al., 2011). In the present study, we have examined the steady-state BTC distribution. Further studies will be needed to determine whether the EExxxL motif directs BTC basolateral delivery and/or recycling. In addition to this dominant EExxxL motif, a palmitoylated cysteine-rich motif (CTCC) serves an accessory role in basolateral sorting of BTC. Disruption of the CTCC motif by itself (C3 mutant) did not alter BTC trafficking. However, when the C3 mutant was combined with the TM mutation (C3/TM), BTC basolateral-sorting fidelity was compromised further, compared to that of the TM mutant alone (Fig. 3). For the CT8 mutant, in addition to reduced basolateral localization, we also observed a reduction in total surface levels, despite overall levels that were comparable to those of wild-type BTC in whole cell lysates. We cannot exclude the possibility that deletion of the entire BTC cytoplasmic domain (and associated palmitoylation) compromises anterograde trafficking through multiple mechanisms, including inefficient maturation or altered N-glycosylation. Cytosolic cysteine residues in EGF-like ligands have recently been shown to regulate their dimerization, which might have implications for their trafficking and/or activity (Hartmann et al.,

2015). A bipartite basolateral-sorting motif is also observed in the cytoplasmic domain of TGFA; however, the specific residues within the dominant basolateral domain (LL versus EExxxL) and accessory juxtamembrane region (HCCQVRKH versus CTCC) differ.

Interestingly, EGFR also has a bipartite basolateral-sorting motif within its cytoplasmic domain; upon disruption of basolateral sorting, extracellular N-glycosylation acts as an apical-sorting determinant (Hobert et al., 1997). We also confirmed N-glycosylation of BTC; however, unlike EGFR, its removal did not affect apical localization of mutant BTC (supplementary material Fig. S1C).

Induction of lateral lumens in polarized MDCK cells by BTC mistrafficking

The most striking observation during the BTC trafficking studies was the formation of lateral lumens in polarized MDCK cells that expressed mistrafficked forms of BTC in Transwell and 3D Matrigel cultures. Hepatocytes form bile canaliculi that represent networks of lateral lumens, and liver-derived WIF-B cells form lateral lumens *in vitro* (Cohen et al., 2004; Ihrke et al., 1993). The laboratory of A. Musch and co-workers have described the formation of lateral lumens in MDCK cells upon overexpression of a polarity protein, Par1b, in conjunction with Ca^{2+} switch or collagen overlay (Cohen et al., 2004; Cohen and Müsch, 2003; Ojakian et al., 1997; Vega-Salas et al., 1988). In parental MDCK cells, lateral lumens are observed early during polarization and are replaced by apical domains after maturation (Cohen et al., 2007). The infrequent lateral lumens that we observed in parental MDCK cells might indicate regions undergoing epithelial maturation or reorganization. We also observed lateral lumen formation after expression of mistrafficked BTC, but this did not require a Ca^{2+} switch or collagen overlay. In our collagen-overlay assays (which modulates integrin signaling), (C3/TM)BTC–EGFP expression compromised the normal MDCK bilayer phenotype, which could be rescued by inhibition of EGFR (Fig. 7D), suggesting that EGFR and integrin signaling might act antagonistically during this epithelial reorganization.

Mistrafficked AREG and EREG did not enhance lateral lumen formation (supplementary material Fig. S4) (Dempsey et al., 2003; Gephart et al., 2011; Singh et al., 2013). Of the seven EGFR ligands, BTC, along with EREG and HBEGF, also bind to another EGFR family member, ERBB4. However, of these, only BTC and HBEGF contain the EExxxL trafficking motif (Singh and Coffey, 2014b). HBEGF in turn does not contain the juxtamembrane cytosolic cysteine residues and has not been shown to undergo regulated intramembranous proteolysis, unlike BTC (Stoeck et al., 2010). Moreover, ligands differ in their affinity for the receptor and in their ability to direct receptors to different intracellular compartments after ligand binding; both of these properties might contribute to the varying effects of the different ligands (Roepstorff et al., 2009).

Finally, the penetrance of the lateral lumen phenotype induced by BTC mutants was not complete; in spite of homogenous BTC expression, lateral lumens were associated with only ~10% of (C3/TM)BTC–EGFP-expressing cells at day 5. Longer culture periods further increased the size and number of lateral lumens. Also, lateral lumens were more abundant in multilayered regions. Another possibility might be that BTC mistrafficking does not initiate the process itself, it only enhances the formation or inhibits the dissolution of infrequent lateral lumens that arise spontaneously.

Another distinctive feature of mistrafficked-BTC-induced lateral lumens is that they coexist with an apical surface at the apex that has a normal appearance (schematic Fig. 7E). We have shown this by locating a number of apical and basolateral markers, and also by examining actin stress fibers, microtubule organization and centriole localization (Figs 4, 6; supplementary material Fig. S2). The simultaneous expression of both apical domains (the apical surface at the apex and lateral lumens) resembles a phenotype observed in individuals with atypical microvillus inclusion disease, which is the result of germline inactivating mutations in syntaxin 3 (Wiegerinck et al., 2014). Another similarity between these two phenotypes is the multilayering of the epithelium (Fig. 5B) (Wiegerinck et al., 2014). Interestingly, a similar phenotype (formation of microvilli along lateral membranes) has been observed in a knockout of Rab11a, a key component of the apical recycling endosome in intestinal epithelial cells (Knowles et al., 2014). Moreover, our observation that lateral lumens form after the establishment of the apical surface might indicate compromised apical recycling of endocytic vesicles. However, we failed to observe an apical-to-lateral-lumen transcytosis of labeled apical proteins (Fig. 5C). Thus, proteins destined for lateral lumen membranes could be delivered directly and/or transcytosed from basolateral membranes. Because lateral lumens are encompassed by tight junctions, they are not amenable to classic surface-labeling and trafficking protocols. Par1b overexpression induces a tilt in the cell division plane with one spindle pole orienting towards the apex, which leads to lateral lumen formation (Lazaro-Dieguez et al., 2013). Our findings that primary cilia localize to the lateral lumens and that multilayering occurs in older cultures, combined with the observation that spindle poles orient towards lateral lumens, might indicate defects in spindle orientation and cell division (Fig. 5B, Fig. 6D; supplementary material Fig. S2C). In addition to Par1b and syntaxin 3, integrin and RhoA signaling have also been implicated in lateral lumen formation (Lazaro-Dieguez et al., 2013; Zuk and Matlin, 1996). Because multilayering and lateral lumens are closely linked, multilayering might itself be contributing to the lateral lumen phenotype by forcing basal cells to generate lateral lumens in an attempt to form an apical surface. Our findings warrant closer scrutiny of the cross-talk between EGFR signaling and these pathways.

Four lateral lumens per 500 cells are present in parental MDCK monolayers under steady-state conditions. The frequency of lateral lumens increases during epithelial reorganization as a consequence of aberrant gene transcription (such as those encoding Par1b and syntaxin 3) or through strong reorientation cues, such as Ca^{2+} switch and collagen overlay, which induce epithelial reorganization; over time, lateral lumens usually disappear or convert into apical domains at the apex (Cohen et al., 2004; Cohen and Müsch, 2003; Ojakian et al., 1997; Vega-Salas et al., 1988; Wiegerinck et al., 2014). Because BTC-induced lateral lumens are structurally similar to parental MDCK lateral lumens and do not collapse after 7 days in culture, we speculate that aberrant EGFR signaling might enhance the *de novo* formation of lateral lumens and/or inhibit their dissolution or conversion into apical domains (Fig. 6D; supplementary material Movies 1–4).

This study further underscores the cell biology that has been uncovered by studying the trafficking of each of the EGFR ligands in polarized epithelial cells (Singh and Coffey, 2014b). For example, basolateral delivery of TGFA depends on the Wnt negative regulator NKD2, providing a point of convergence between EGFR-related events and Wnt signaling (Li et al., 2004). Studies of HBEGF trafficking have led to the discovery that EGFR ligands can be packaged and released in the form of exosomes (Higginbotham et al., 2011). The present results identify a unique phenotype of BTC mistrafficking – induction of EGFR-

Journal of Cell Science (2015) 128, 3444-3455 doi:10.1242/jcs.170852

dependent lateral lumen formation. Moreover, we recapitulated the lateral lumen phenotype with a human cancer-associated BTC mistrafficking mutation. The enhanced growth phenotype associated with the mistrafficking forms of BTC, including the cancer-associated mutation, underscores the biological significance of these studies. The possible clinical importance of these findings awaits further investigation.

MATERIALS AND METHODS

Chemicals and reagents

All chemicals were purchased from Sigma-Aldrich unless stated otherwise. All cell culture media and supplements were purchased from Gibco Laboratories, except bovine growth serum, which was purchased from HyClone Laboratories. Biotin (EZ-Link Sulfo-NHS-LC-Biotin) was purchased from Pierce Biotechnology. EKI-785 was obtained from Philip Frost (Wyeth-Ayerst). G418, Protein G agarose, Rhodamine–phalloidin and HRP–streptavidin were purchased from Invitrogen.

Antibodies

Anti-GFP (catalog no. A11122) and anti-ZO-1 (catalog no. 61-7300) antibodies were purchased from Invitrogen. Anti-gp135 mouse monoclonal antibody was kindly provided by James R. Goldenring (Vanderbilt University, Nashville, TN). Anti-ezrin antibody was purchased from Cell Signaling (catalog no. 3145) and anti-Na^+/K^+-transporting ATPase α1 antibody was purchased from Abcam (catalog no. Ab76020). Fluorescent secondary antibodies were purchased from Jackson ImmunoResearch Laboratories. Secondary antibodies (TrueBlot) for western blotting were purchased from eBioscience. The mouse monoclonal antibody against human AREG (clone 6R1C2.4) has been described previously (Brown et al., 1998; Gephart et al., 2011).

Cell culture

All reagents for cell culture were purchased from Gibco Laboratories unless otherwise stated. MDCK (type II) cells were obtained from Enrique Rodriguez-Boulan (Weill Cornell Medical College, New York, NY). These cells were propagated in Dulbecco's modified Eagle's medium containing 10% bovine growth serum, supplemented with non-essential amino acids, L-glutamine 2 mM, penicillin (100 U/ml) and streptomycin (100 µg/ml) in an incubator maintained at 37°C, 5% CO_2 and 90% humidity. Cell culture medium was replenished every other day. MDCK cells stably expressing TGFA, AREG and EREG constructs have been described previously (Dempsey et al., 2003; Gephart et al., 2011; Singh et al., 2013).

Polarized epithelial culture

For polarized MDCK cultures, 100,000 cells were seeded on the inner side of 12-mm Transwell inserts (polycarbonate, 0.4 µm, Corning) in 0.5 ml of serum-supplemented DMEM medium; the outer lower chamber was supplemented with 1.5 ml of medium. Transwell cultures at days 4 to 5 usually showed a TEER measurement of more than 200 Ω cm^2; cultures above this threshold were considered polarized. TEER was measured using a Millicell ERS-2 Voltohmmeter by EMD Millipore. Polarity was further confirmed by staining for tight junctions with ZO-1 and apical staining above the tight junctions for proteins like gp135 and ezrin.

EGFR inhibition (treatment with EKI-785)

A stock solution of EKI-785 that had been dissolved in DMSO was diluted in serum-supplemented DMEM at a concentration of 2 µM. Medium from both apical and basal compartments of MDCK cells plated on Transwell filters was replaced with EKI-785-supplemented medium on day 3. Cells were typically harvested on day 5; for longer incubations, EKI-785-supplemented medium was replaced every other day.

BTC cloning and expression

The complete coding region of BTC was amplified from an mRNA clone obtained from the Vanderbilt Microarray Shared Resource and was cloned into the Clontech vector pEGFP-N1 (GenBank U55762.1) between the *Kpn*1–*Xma*1 restriction sites within the multiple cloning site of the vector in frame with downstream EGFP. Cytoplasmic domain truncations and amino acid substitutions were subsequently derived from this construct. Four hundred thousand MDCK cells were transfected with 1 µg of plasmid using Metafectene Pro (Biontex Laboratories GmbH, Germany). A day after transfection, cells were subjected to selection with G418 (1 mg/ml) for 10 days and cloned by fluorescence-activated cell sorting for GFP fluorescence. Stable BTC-expressing clones were maintained in 300 µg/ml of G418, which was removed before starting experiments.

Immunofluorescence and confocal microscopy

For routine staining, MDCK cells that had polarized on Transwell filters were washed three times with cold PBS, fixed with 4% paraformaldehyde (PFA) in PBS for 30 min at 4°C, washed three times with cold PBS, and permeabilized with immunofluorescence buffer (0.1% BSA, 0.1% Triton X-100 in PBS) for 6–24 h at 4°C. Cells were blocked with 3% normal donkey serum in immunofluorescence buffer for 2 h at room temperature. Subsequent incubation with primary antibody (diluted in immunofluorescence buffer, 1 h), washes (three times with immunofluorescence buffer, 15 min each), secondary antibody (diluted in immunofluorescence buffer, 1 h) and final washes (three times with immunofluorescence buffer, 15 min each) were all performed at room temperature. DAPI and Rhodamine–phalloidin were added in the secondary antibody incubation step. Filters cut out of Transwell inserts were mounted in Prolong Gold anti-fade mounting medium (Life Technologies). Most images were acquired with a Carl Zeiss LSM 710 confocal microscope using a 63× objective; all *z*-stacks were imaged at 1024×1024 resolution, 2× zoom with *z*-slice interval set at 0.5 µm, unless specified otherwise. A minority of the confocal images were acquired with a Nikon A1R confocal microscope using a 60× objective, at 1024×1024 resolution, 2× zoom with *z*-slice interval set at 0.5 µm, unless specified otherwise. Analysis and 3D reconstruction were performed using Carl Zeiss software ZEN 2012 SP1 or Nikon software NIS-Elements. Images were further processed and compiled in Adobe Photoshop CS4 and/or CorelDraw X6.

MDCK Matrigel cultures

The MDCK Matrigel culture method was adapted from a previous publication (Bryant et al., 2010). Briefly, each chamber of an eight-chamber Coverglass System (Lab-Tek Cat. 115411) was uniformly coated with 5 µl of Matrigel. On these coated chambers, 4000 MDCK cells were added on top as a single cell suspension in 400 µl of DMEM supplemented with 5% serum and 2% Matrigel. Individual cells grew to form cysts within 4–6 days, which were then fixed with 4% PFA for 5 min at room temperature and subjected to immunofluorescence and microscopy analyses as described above.

Selective cell surface biotinylation

Polarized MDCK cells on 12-mm Transwell filters were washed three times with ice-cold PBS supplemented with 0.1 mM $CaCl_2$ and 1.0 mM $MgCl_2$ (PBS-CM). Biotin stocks were prepared at 200 mg/ml in anhydrous DMSO and stored at −20°C. A working concentration of 0.5 mg/ml biotin was prepared fresh in ice-cold PBS-CM from these stocks. For apical biotinylation, 0.5 ml of biotin-supplemented PBS-CM was added to the inner compartment of Transwell filters, and 1.5 ml of PBS-CM was added to the outer compartment. For basolateral biotinylation, the order was reversed; the basolateral compartment received 1.5 ml of biotin-supplemented PBS-CM instead. After a 20-min incubation at 4°C, Transwell filters were replaced with fresh biotin and incubated for another 20 min at 4°C. Biotin was then quenched with five washes of PBS-CM containing 100 mM glycine and 0.2% BSA at 4°C. To remove glycine, another two washes with PBS-CM were performed at 4°C. Filters were then cut out of the Transwell inserts and added to Eppendorf tubes containing 600 µl of lysis buffer and rotated gently for 30 min at 4°C. Filters were then removed, and the lysates were centrifuged for 15 min at 18,000 ***g*** in a tabletop cooling centrifuge; supernatants were then collected in separate tubes and processed for subsequent western blot analysis.

Collagen-overlay assays

Four-day-old MDCK Transwell cultures were washed twice with warm PBS. Fifty microliters of 1.5 mg/ml bovine collagen in serum-supplemented DMEM was added on top of filters and placed in the incubator for 10 min to polymerize. After collagen polymerization, growth medium was added on top of the filters; EKI-785 (2 µM) was added to both sides of the filters where indicated. Cultures were then allowed to grow for an additional 48 h, and fixed and processed for immunofluorescence as described above.

Cell lysis, immunoprecipitation and immunoblotting

Lysis buffer composition: 50 mM HEPES (pH 7.5), 150 mM NaCl, 1% Triton X-100, 1 mM EDTA, 10% glycerol and 10 mM sodium pyrophosphate; 2 mM sodium orthovanadate, 10 mM sodium fluoride, 1 mM PMSF, 5 µg/ml leupeptin, 5 µg/ml pepstatin and 10 µg/ml aprotinin were added separately before lysis. Lysis was performed for 30 min at 4°C. Lysates were pre-cleared by centrifuging at 18,000 ***g*** for 15 min at 4°C in a tabletop cooling centrifuge. Protein concentration was estimated using bicinchoninic acid (BCA) protein assay (Pierce Biotechnology). For western blot analysis, samples with equal amounts of protein were mixed 1:1 with 2× Laemmli buffer (containing 5% β-mercaptoethanol), boiled for 5 min, resolved on 10% SDS-PAGE, and subsequently electrophoretically transferred onto nitrocellulose membranes. The membranes were blocked with 5% milk in Tris-buffered saline containing 0.1% Tween-20 (TBST); biotinylation blots were blocked with 5% BSA in TBST instead. Primary and secondary antibodies were diluted in the blocking buffer. Blots were stripped in 65 mM Tris (pH 6.8) containing 2% SDS and 0.8% β-mercaptoethanol for 45 min at 50°C, washed with TBST (at least ten times) and blocked for subsequent immunoblotting. For immunoprecipitations, lysates were pre-cleared with protein G agarose beads overnight at 4°C. Fresh beads and appropriate antibodies were added in the immunoprecipitation dilution buffer (4× HNTG: 200 mM HEPES, pH 7.5, 600 mM NaCl, 40% glycerol and 0.4% Triton X-100) and incubated with cleared lysates for 4 h at 4°C with gentle agitation. Beads were then washed three times in 600 µl of HNTG buffer and resuspended in 30 µl of 2× Laemmli buffer, and subjected to SDS-PAGE followed by western blot analysis.

Transmission electron microscopy

Specimens were processed for TEM and imaged in the Vanderbilt Cell Imaging Shared Resource. All fixations, staining and washes were performed in 0.1 M cacodylate buffer, pH 7.4 at room temperature. MDCK cells that had been polarized on Transwell filters were fixed in 2.5% glutaraldehyde for 1 h. Samples were stained with 1% osmium tetraoxide for 1 h. After washing away the excess stain, samples were dehydrated through a series of graded ethanol washes followed by three exchanges of 100% ethanol and two exchanges of pure propylene oxide. For Epon 812 resin infiltration, samples were sequentially incubated with 25% resin for 30 min, 50% resin for 1 h in propylene oxide, followed by incubation with pure resin 48 h at room temperature. Samples were then allowed to polymerize at 60°C for 48 h. Thick sections (500 nm to 1 µm) were collected using a Leica Ultracut microtome, contrast stained with 1% Toluidine Blue, and imaged with a Nikon AZ100 microscope. Ultra-thin sections (70–80 nm) were cut and collected on 300-mesh copper grids and post-stained with 2% uranyl acetate and then with Reynold's lead citrate, and imaged on the Philips/FEI Tecnai T12 electron microscope at various magnifications.

Quantification of lateral lumens

MDCK Transwell cultures that had been stained for ZO-1, DAPI and gp135 were imaged at five microns above the base at 1024×1024 resolution that covered 224.92×224.92 µm at 0.5 µm *z*-slice. Images in the gp135-detection channel were used to quantify the number and size of lateral lumens using ImageJ. The macro indicating the conditions is pasted as follows: run ("Gaussian Blur…," "sigma=15 slice)"; ¶ setAutoThreshold("Default dark)"; ¶ //run("Threshold…)"; ¶ setThreshold(50, 255); ¶ run("Convert to Mask," "method=Default background=Dark black)"; ¶ run("Analyze Particles…," "circularity=0.50-1.00 show=Outlines display exclude include slice)"; ¶saveAs("Tiff," "C:\\Users\\singhb1\\Desktop\\LLQ\ \MDCK- 1M.tif)"; ¶ String.copyResults(); ¶ close(); ¶ close();¶ close();

Quantification of western blots

Western blot densitometry analysis was performed with ImageJ analysis software (National Institutes of Health) as per the developer's instructions. % basolateral=([BL]/[Ap]+[BL])×100 (where BL, basolateral; Ap, apical). Results are displayed as the mean of at least three independent experiments ±s.e.m.

Statistical analysis

Five random areas from the Transwell cultures were chosen for quantification of the lateral lumens. The average number and area of lateral lumens was compared using a two-tailed unpaired *t*-test.

Acknowledgements

We thank Jim Higginbotham for FACS-based cloning of MDCK cells expressing various BTC–EGFP constructs. We thank Eliot McKinley for help with optimization of parameters for ImageJ image analysis. We thank Daniel Albarran, DingDing Shen and Julia Allen for help with generating reagents. We thank Emily J. Poulin for editing the manuscript. We acknowledge the support of the Flow Cytometry and Cell Imaging Shared Resources provided by the Vanderbilt-Ingram Cancer Center and Vanderbilt's Digestive Disease Research Center.

Competing interests

The authors declare no competing or financial interests.

Author contributions

B.S., G.B., A.S., J.R.G. and R.J.C. designed research; B.S., G.B., A.S., J.S., L.A.L. and J.A.W. performed research; B.S., J.R.G. and R.J.C. analyzed data and provided critical input; and B.S. and R.J.C. wrote the paper.

Funding

This work was supported by National Institutes of Health (NIH) [grant numbers R01-CA46413 and P50-CA95103 to R.J.C., and R01-DK48370 and R01-DK70856 to J.R.G]. Deposited in PMC for release after 12 months.

Supplementary material

Supplementary material available online at http://jcs.biologists.org/lookup/suppl/doi:10.1242/jcs.170852/-/DC1

References

Brown, C. L., Meise, K. S., Plowman, G. D., Coffey, R. J. and Dempsey, P. J. (1998). Cell surface ectodomain cleavage of human amphiregulin precursor is sensitive to a metalloprotease inhibitor. Release of a predominant N-glycosylated 43-kDa soluble form. *J. Biol. Chem.* **273**, 17258-17268.

Brown, C. L., Coffey, R. J. and Dempsey, P. J. (2001). The proamphiregulin cytoplasmic domain is required for basolateral sorting, but is not essential for constitutive or stimulus-induced processing in polarized Madin-Darby Canine kidney cells. *J. Biol. Chem.* **276**, 29538-29549.

Bryant, D. M. and Mostov, K. E. (2008). From cells to organs: building polarized tissue. *Nat. Rev. Mol. Cell Biol.* **9**, 887-901.

Bryant, D. M., Datta, A., Rodríguez-Fraticelli, A. E., Peränen, J., Martín-Belmonte, F. and Mostov, K. E. (2010). A molecular network for de novo generation of the apical surface and lumen. *Nat. Cell Biol.* **12**, 1035-1045.

Cerami, E., Gao, J., Dogrusoz, U., Gross, B. E., Sumer, S. O., Aksoy, B. A., Jacobsen, A., Byrne, C. J., Heuer, M. L., Larsson, E. et al. (2012). The cBio cancer genomics portal: an open platform for exploring multidimensional cancer genomics data. *Cancer Discov.* **2**, 401-404.

Cohen, D. and Müsch, A. (2003). Apical surface formation in MDCK cells: regulation by the serine/threonine kinase EMK1. *Methods* **30**, 269-276.

Cohen, D., Brennwald, P. J., Rodriguez-Boulan, E. and Müsch, A. (2004). Mammalian PAR-1 determines epithelial lumen polarity by organizing the microtubule cytoskeleton. *J. Cell Biol.* **164**, 717-727.

Cohen, D., Tian, Y. and Musch, A. (2007). Par1b promotes hepatic-type lumen polarity in Madin Darby canine kidney cells via myosin II- and E-cadherin-dependent signaling. *Mol. Biol. Cell* **18**, 2203-2215.

Dahlhoff, M., Wolf, E. and Schneider, M. R. (2014). The ABC of BTC: structural properties and biological roles of betacellulin. *Semin. Cell Dev. Biol.* **28**, 42-48.

Dempsey, P. J., Meise, K. S., Yoshitake, Y., Nishikawa, K. and Coffey, R. J. (1997). Apical enrichment of human EGF precursor in Madin-Darby canine kidney cells involves preferential basolateral ectodomain cleavage sensitive to a metalloprotease inhibitor. *J. Cell Biol.* **138**, 747-758.

Dempsey, P. J., Meise, K. S. and Coffey, R. J. (2003). Basolateral sorting of transforming growth factor-alpha precursor in polarized epithelial cells: characterization of cytoplasmic domain determinants. *Exp. Cell Res.* **285**, 159-174.

Discafani, C. M., Carroll, M. L., Floyd, M. B., Jr, Hollander, I. J., Husain, Z., Johnson, B. D., Kitchen, D., May, M. K., Malo, M. S., Minnick, A. A.Jr et al. (1999). Irreversible inhibition of epidermal growth factor receptor tyrosine kinase with in vivo activity by N-[4-[(3-bromophenyl)amino]-6-quinazolinyl]-2-butynamide (CL-387,785). *Biochem. Pharmacol.* **57**, 917-925.

Gephart, J. D., Singh, B., Higginbotham, J. N., Franklin, J. L., Gonzalez, A., Fölsch, H. and Coffey, R. J. (2011). Identification of a novel mono-leucine basolateral sorting motif within the cytoplasmic domain of amphiregulin. *Traffic* **12**, 1793-1804.

Groenestege, W. M. T., Thébault, S., van der Wijst, J., van den Berg, D., Janssen, R., Tejpar, S., van den Heuvel, L. P., van Cutsem, E., Hoenderop, J. G., Knoers, N. V. et al. (2007). Impaired basolateral sorting of pro-EGF causes isolated recessive renal hypomagnesemia. *J. Clin. Invest.* **117**, 2260-2267.

Harris, R. C., Chung, E. and Coffey, R. J. (2003). EGF receptor ligands. *Exp. Cell Res.* **284**, 2-13.

Hartmann, M., Parra, L. M., Ruschel, A., Lindner, C., Morrison, H., Herrlich, A. and Herrlich, P. (2015). Inside-out regulation of ectodomain cleavage of cluster-of-differentiation-44 (CD44) and of neuregulin-1 requires substrate dimerization. *J. Biol. Chem.* **290**, 17041-17054.

Higginbotham, J. N., Demory Beckler, M., Gephart, J. D., Franklin, J. L., Bogatcheva, G., Kremers, G.-J., Piston, D. W., Ayers, G. D., McConnell, R. E., Tyska, M. J. et al. (2011). Amphiregulin exosomes increase cancer cell invasion. *Curr. Biol.* **21**, 779-786.

Hobert, M. E., Kil, S. J., Medof, M. E. and Carlin, C. R. (1997). The cytoplasmic juxtamembrane domain of the epidermal growth factor receptor contains a novel autonomous basolateral sorting determinant. *J. Biol. Chem.* **272**, 32901-32909.

Ihrke, G., Neufeld, E. B., Meads, T., Shanks, M. R., Cassio, D., Laurent, M., Schroer, T. A., Pagano, R. E. and Hubbard, A. L. (1993). WIF-B cells: an in vitro model for studies of hepatocyte polarity. *J. Cell Biol.* **123**, 1761-1775.

Knowles B. C., Weis, V. G., Yu, S., Roland, J.T., Williams, J. A., Alvarado, G. S., Lapierre, L. A., Shub, M. D., Gao, N. and Goldenring, J. R. (2015). Rab11a regulates syntaxin 3 localization and microvillus assembly in enterocytes. *J. Cell Sci.* **128**, 1617-1626.

Lazaro-Dieguez, F., Cohen, D., Fernandez, D., Hodgson, L., van Ijzendoorn, S. C. D. and Musch, A. (2013). Par1b links lumen polarity with LGN-NuMA positioning for distinct epithelial cell division phenotypes. *J. Cell Biol.* **203**, 251-264.

Li, C., Franklin, J. L., Graves-Deal, R., Jerome, W. G., Cao, Z. and Coffey, R. J. (2004). Myristoylated Naked2 escorts transforming growth factor alpha to the basolateral plasma membrane of polarized epithelial cells. *Proc. Natl. Acad. Sci. USA* **101**, 5571-5576.

Mellman, I. and Nelson, W. J. (2008). Coordinated protein sorting, targeting and distribution in polarized cells. *Nat. Rev. Mol. Cell Biol.* **9**, 833-845.

Nakamura, K., Iwamoto, R. and Mekada, E. (1995). Membrane-anchored heparin-binding EGF-like growth factor (HB-EGF) and diphtheria toxin receptor-associated protein (DRAP27)/CD9 form a complex with integrin alpha 3 beta 1 at cell-cell contact sites. *J. Cell Biol.* **129**, 1691-1705.

Ojakian, G. K., Nelson, W. J. and Beck, K. A. (1997). Mechanisms for de novo biogenesis of an apical membrane compartment in groups of simple epithelial cells surrounded by extracellular matrix. *J. Cell Sci.* **110**, 2781-2794.

Rodriguez-Boulan, E. and Macara, I. G. (2014). Organization and execution of the epithelial polarity programme. *Nat. Rev. Mol. Cell Biol.* **15**, 225-242.

Roepstorff, K., Grandal, M. V., Henriksen, L., Knudsen, S. L. J., Lerdrup, M., Grøvdal, L., Willumsen, B. M. and van Deurs, B. (2009). Differential effects of EGFR ligands on endocytic sorting of the receptor. *Traffic* **10**, 1115-1127.

Sahin, U., Weskamp, G., Kelly, K., Zhou, H.-M., Higashiyama, S., Peschon, J., Hartmann, D., Saftig, P. and Blobel, C. P. (2004). Distinct roles for ADAM10 and ADAM17 in ectodomain shedding of six EGFR ligands. *J. Cell Biol.* **164**, 769-779.

Scheiffele, P., Peränen, J. and Simons, K. (1995). N-glycans as apical sorting signals in epithelial cells. *Nature* **378**, 96-98.

Schneider, M. R., Antsiferova, M., Feldmeyer, L., Dahlhoff, M., Bugnon, P., Hasse, S., Paus, R., Wolf, E. and Werner, S. (2008). Betacellulin regulates hair follicle development and hair cycle induction and enhances angiogenesis in wounded skin. *J. Invest. Dermatol.* **128**, 1256-1265.

Singh, B. and Coffey, R. J. (2014a). From wavy hair to naked proteins: the role of transforming growth factor alpha in health and disease. *Semin. Cell Dev. Biol.* **28**, 12-21.

Singh, B. and Coffey, R. J. (2014b). Trafficking of epidermal growth factor receptor ligands in polarized epithelial cells. *Annu. Rev. Physiol.* **76**, 275-300.

Singh, B., Bogatcheva, G., Washington, M. K. and Coffey, R. J. (2013). Transformation of polarized epithelial cells by apical mistrafficking of epiregulin. *Proc. Natl. Acad. Sci. USA* **110**, 8960-8965.

Stoeck, A., Shang, L. and Dempsey, P. J. (2010). Sequential and gamma-secretase-dependent processing of the betacellulin precursor generates a palmitoylated intracellular-domain fragment that inhibits cell growth. *J. Cell Sci.* **123**, 2319-2331.

Vega-Salas, D. E., Salas, P. J. and Rodriguez-Boulan, E. (1988). Exocytosis of vacuolar apical compartment (VAC): a cell-cell contact controlled mechanism for the establishment of the apical plasma membrane domain in epithelial cells. *J. Cell Biol.* **107**, 1717-1728.

Vermeer, P. D., Einwalter, L. A., Moninger, T. O., Rokhlina, T., Kern, J. A., Zabner, J. and Welsh, M. J. (2003). Segregation of receptor and ligand regulates activation of epithelial growth factor receptor. *Nature* **422**, 322-326.

Wiegerinck, C. L., Janecke, A. R., Schneeberger, K., Vogel, G. F., van Haaften-Visser, D. Y., Escher, J. C., Adam, R., Thöni, C. E., Pfaller, K., Jordan, A. J. et al. (2014). Loss of syntaxin 3 causes variant microvillus inclusion disease. *Gastroenterology* **147**, 65-68.e10.

Zuk, A. and Matlin, K. S. (1996). Apical beta 1 integrin in polarized MDCK cells mediates tubulocyst formation in response to type I collagen overlay. *J. Cell Sci.* **109**, 1875-1889.

SUPPLEMENTARY MATERIAL

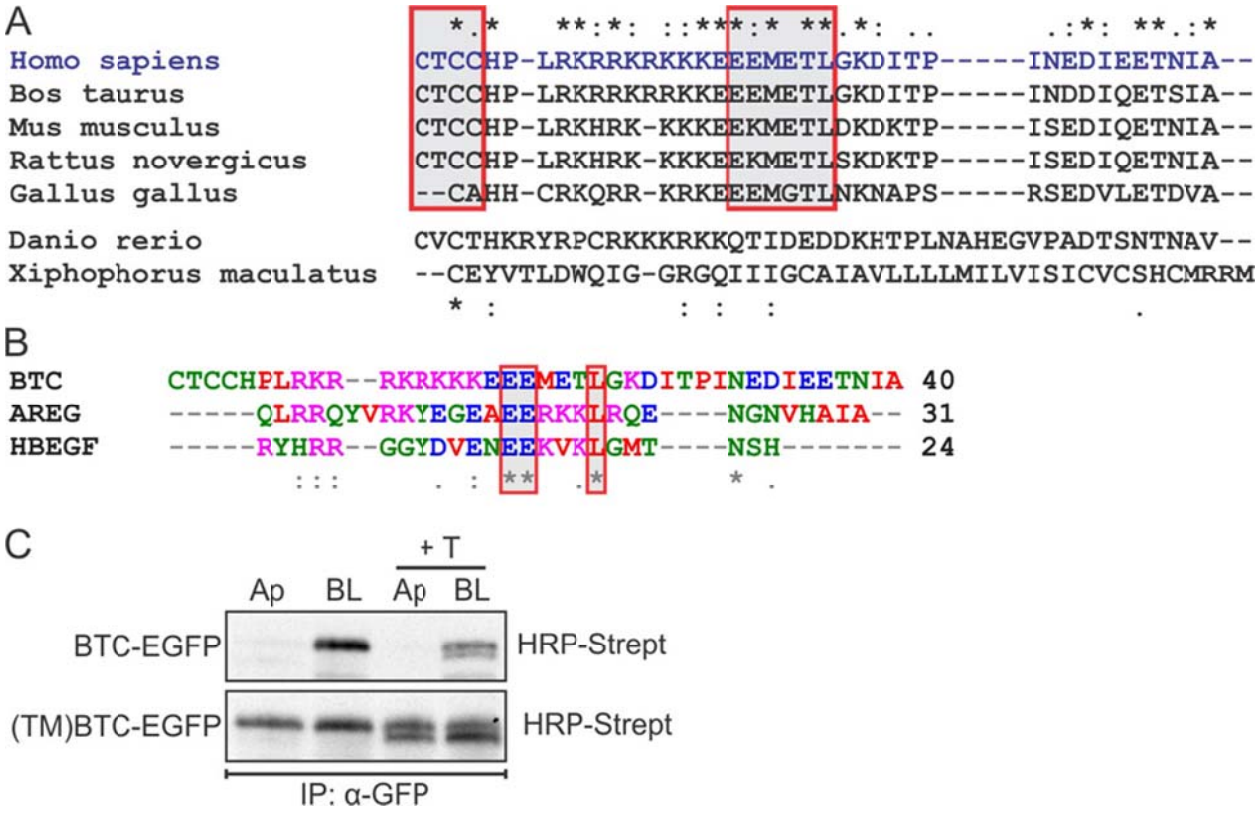

Fig. S1. BTC Cytoplasmic domain alignment and the role of N-glycosylation in BTC trafficking. (A) Cross-species alignment of BTC cytoplasmic domain: the regions showing high sequence homology are shaded in a box with the alignment scores displayed above each aligned aa. * indicates absolutely conserved residues followed by : and . in decreasing order of homology. (B) Conservation of the monoleucine-based basolateral-sorting motif (EEXXXL) within the cytoplasmic domain of AREG, BTC, and HBEGF: the key monoleucine and proximal acidic aa in the basolateral-sorting motif are conserved. (C) BTC N-glycosylation is not required for its apical localization: MDCK cells stably expressing BTC-EGFP and (TM)BTC-EGFP were polarized on Transwell filters and subjected to selective cell-surface biotinylation on either apical (Ap) or basolateral (BL) cell surfaces. A separate pair of filters for each line were preincubated with an N-glycosylation inhibitor, Tunicamycin (2 mg/ml), for 9 hours (+T) and subjected to selective cell-surface biotinylation. Cells were then lysed, immunoprecipitated for GFP, and probed with HRP-streptavidin.

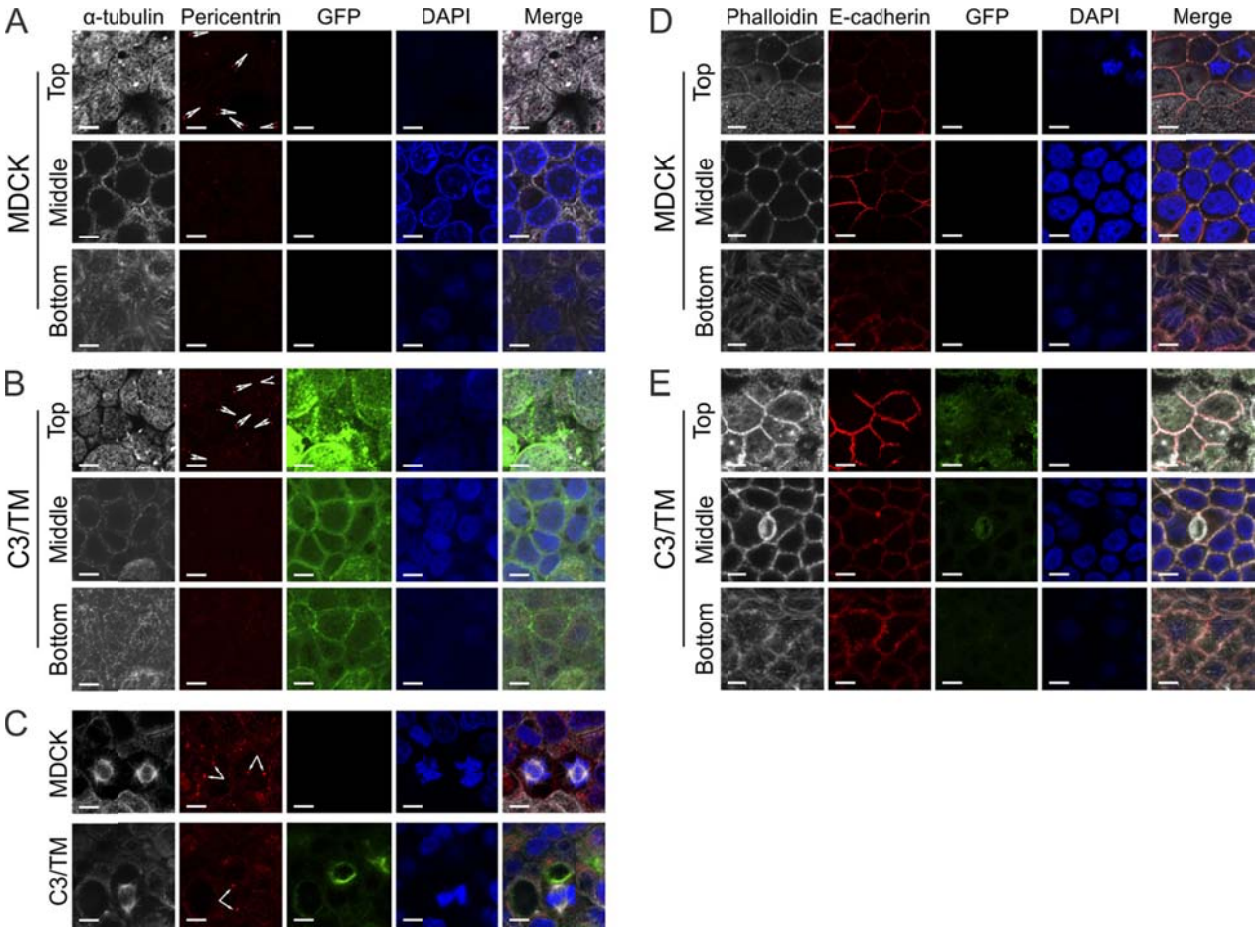

Fig. S2. Cytoskeletal organization of parental and C3/TM-expressing MDCK Transwell cultures. (A) Polarized MDCK were fixed and stained for DAPI (blue), α-tubulin (white), and pericentrin (red). Three xy projections at the top, midde, and bottom position of the Transwell cultures are shown. Pericentrin-stained centrioles in individual cells are indicated with a pair of arrows. (B) Polarized MDCK cells stably expressing (C3/TM)BTC-EGFP were fixed, stained, and displayed as in A. (C) Dividing cells within parental or (C3/TM)BTC-EGFP-expressing MDCK Transwell cultures were fixed and stained as in A. xy projection through the division plane are displayed. (D) Polarized MDCK were fixed and stained for DAPI (blue), phalloidin (white), and E-cadherin (red). Three xy projections at the top, middle, and bottom position of the Transwell cultures are shown. (E) Polarized MDCK cells stably expressing (C3/TM)BTC-EGFP were fixed, stained, and displayed as in D. All scale bars: 10 μm.

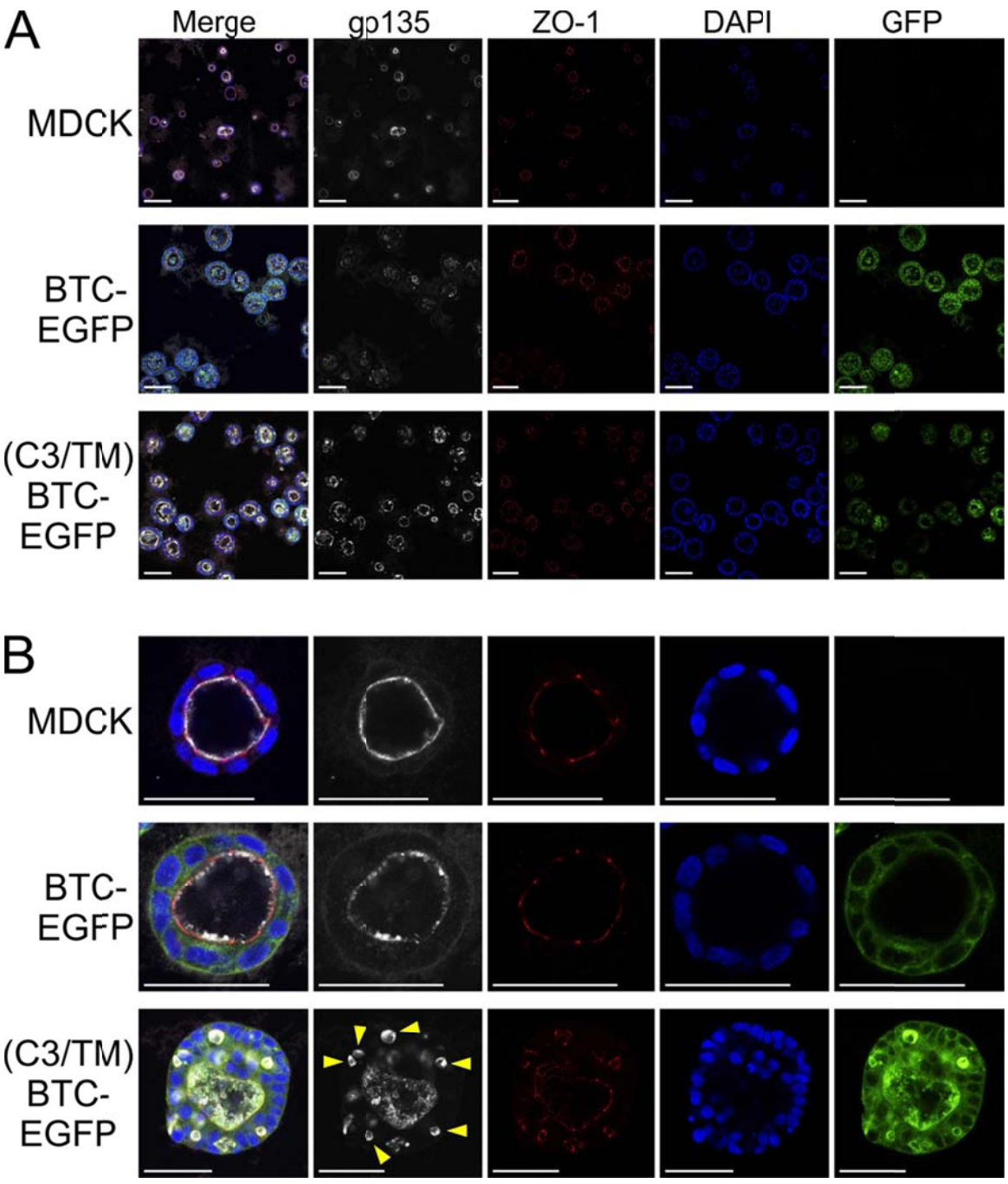

Fig. S3. BTC mistrafficking enhances lateral lumen formation in 3D cultures. (A, B) MDCK cells stably expressing the indicated BTC constructs were cultured in Matrigel for five days and then fixed and stained for ZO-1 (red) and gp135 (white). GFP and DAPI fluorescence are depicted in green and blue, respectively. Both low (A) and high (B) power xy projections show multiple and individual cysts, respectively. Yellow arrowheads in gp135 channel in B indicate lateral lumens. Scale bars: A = 100 μm, B = 50 μm.

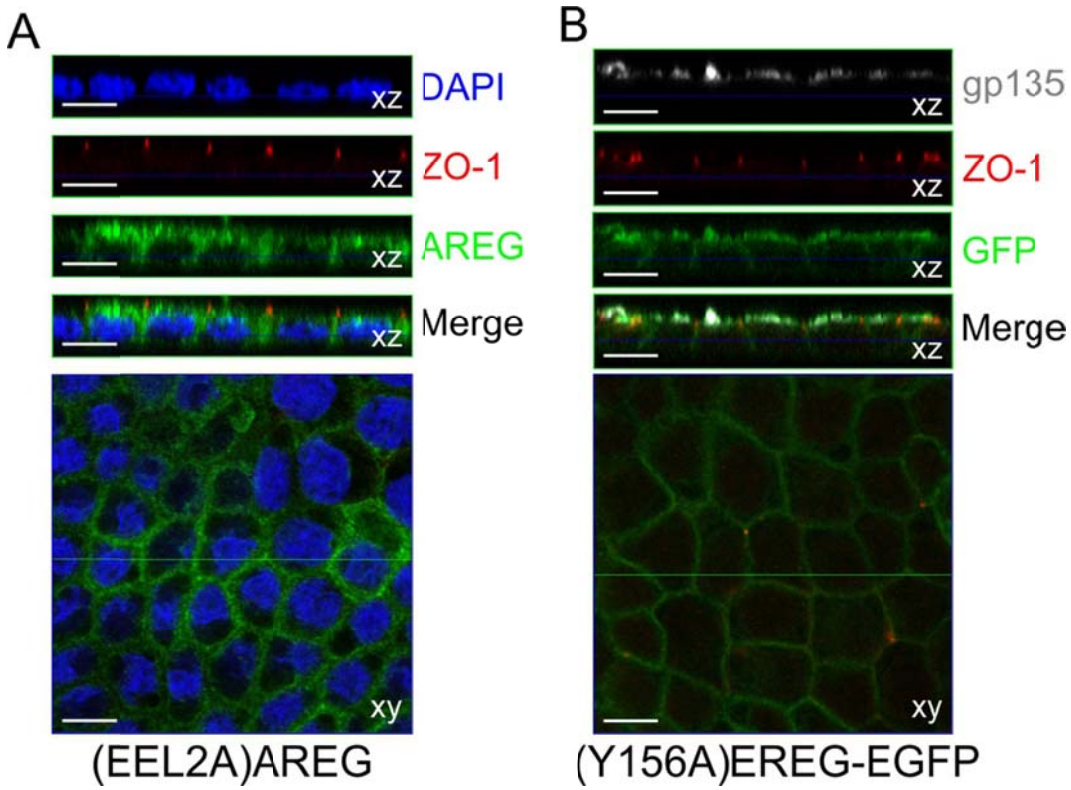

Fig. S4. AREG and EREG mistrafficking does not induce lateral lumens in MDCK cells. (A) Polarized MDCK cells stably expressing the AREG mistrafficking mutant, (EEL2A)AREG, were fixed and immunostained for AREG (green) and ZO-1 (red) and stained for DAPI (blue). (B) Polarized MDCK cells stably expressing the EREG mistrafficking mutant, (Y156A)EREG-EGFP, were fixed and immunostained for gp135 (white), ZO-1 (red), and stained for DAPI (blue); GFP fluorescence is shown in green. Composite xy projections and xz projections in individual channels are displayed. All scale bars: 10 µm.

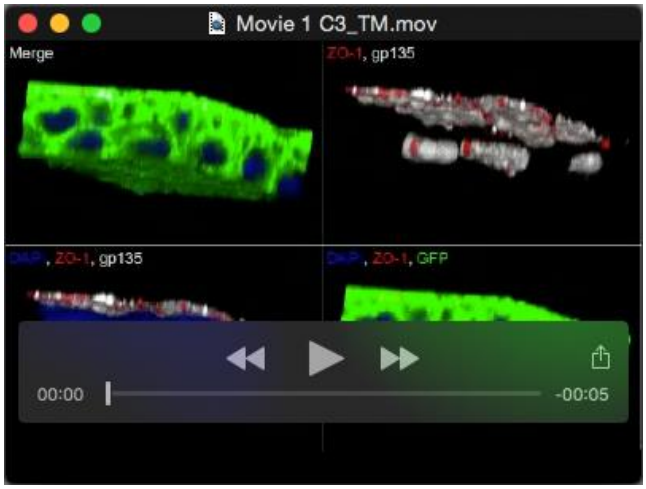

Movie 1. 3D projection of a lateral lumen in (C3/TM)BTC-EGFP-expressing MDCK cells. Polarized MDCK cells stably expressing (C3/TM)BTC-EGFP were fixed and stained for nuclei (DAPI, blue), tight junctions (ZO-1, red), and the apical surface (gp135, white); green color indicates BTC-EGFP fluorescence. A 3D projection of a confocal z-stack containing a lateral lumen is displayed with different combinations of stains.

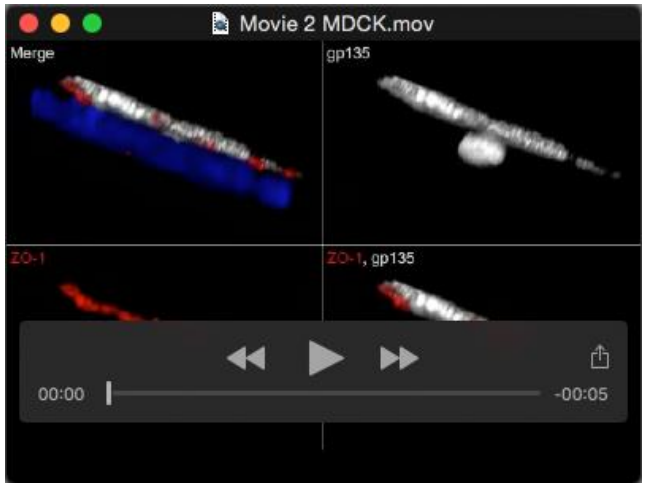

Movie 2. 3D projection of a lateral lumen in parental MDCK cells. Polarized MDCK cells were fixed and stained for nuclei (DAPI, blue), tight junctions (ZO-1, red), and the apical surface (gp135, white). A 3D projection of a confocal z-stack containing a lateral lumen is displayed with different combinations of stains.

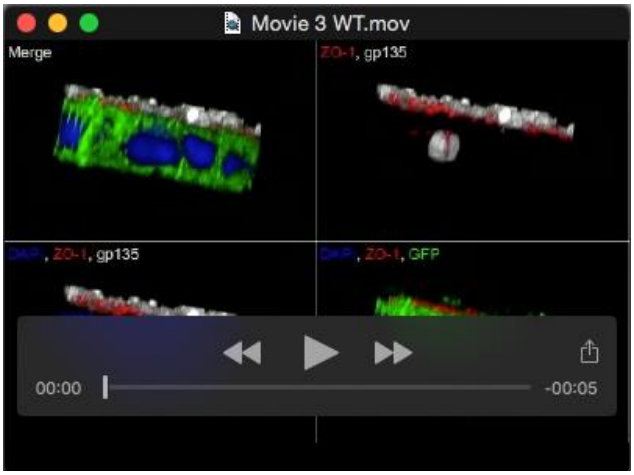

Movie 3. 3D projection of a lateral lumen in BTC-EGFP-expressing MDCK cells. Polarized MDCK cells stably expressing BTC-EGFP were fixed and stained for nuclei (DAPI, blue), tight junctions (ZO-1, red), and the apical surface (gp135, white); green color indicates BTC-EGFP fluorescence. A 3D projection of a confocal z-stack containing a lateral lumen is displayed with different combinations of stains.

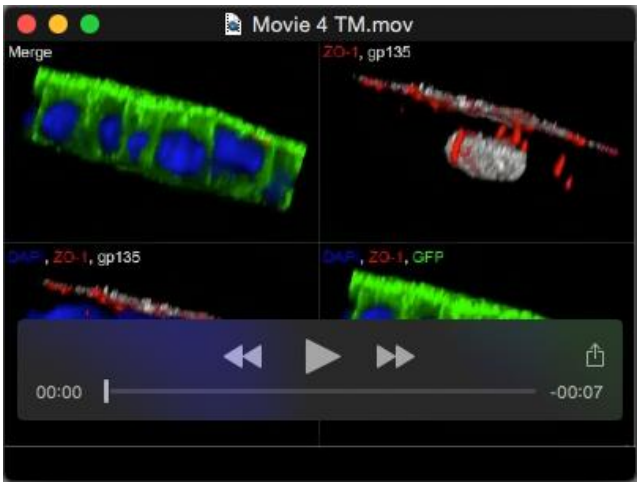

Movie 4. 3D projection of a lateral lumen in (TM)BTC-EGFP-expressing MDCK cells. Polarized MDCK cells stably expressing (TM)BTC-EGFP were fixed and stained for nuclei (DAPI, blue), tight junctions (ZO-1, red), and the apical surface (gp135, white); green color indicates BTC-EGFP fluorescence. A 3D projection of a confocal z-stack containing a lateral lumen is displayed with different combinations of stains.